

Characterization of Three Members of the Electron-Transfer Series $[\text{Fe}(\text{pda})_2]^n$ ($n = 2-, 1-, 0$) by Spectroscopy and Density Functional Theoretical Calculations [pda = Redox Non-innocent Derivatives of N,N' -Bis(pentafluorophenyl)-*o*-phenylenediamide($2-, 1-, 0$)]

Marat M. Khusniyarov,^{*[a, b]} Eckhard Bill,^[a] Thomas Weyhermüller,^[a] Eberhard Bothe,^[a] Klaus Harms,^[b] Jörg Sundermeyer,^{*[b]} and Karl Wieghardt^{*[a]}

Abstract: The four-coordinate iron complexes, $[\text{Fe}^{\text{III}}(\text{pda}^{2-})(\text{pda}^-)]$ (**1**) and $[\text{AsPh}_4]_2[\text{Fe}^{\text{II}}(\text{pda}^{2-})_2]$ (**2**) were synthesized and fully characterized; pda^{2-} is the closed-shell ligand N,N' -bis(pentafluorophenyl)-*o*-phenylenediamido- ($2-$), and pda^- represents its one-electron-oxidized π -radical anion. Single-crystal X-ray diffraction studies of **1** and **2** performed at 100(2) K reveal a distorted tetrahedral coordination environment at the iron centers, as a result of the intramolecular π - π interactions between C_6F_5 rings. The electronic structures of **1** and **2** were unambiguously determined by a combination of ^{57}Fe Mössbauer and electronic spectroscopy, magnetic susceptibility measurements, X-ray crystallography, and

DFT calculations. Compound **1** contains an intermediate-spin Fe^{III} ion ($S_{\text{Fe}} = 3/2$) strongly antiferromagnetically coupled to a π -ligand radical ($S_{\text{R}} = 1/2$) yielding an $S_{\text{t}} = 1$ ground state. Complex **2** possesses a high-spin Fe^{II} center ($S_{\text{Fe}} = 2$) with two closed-shell dianionic ligands. Complexes **1** and **2** are members of the redox series $[\text{Fe}(\text{pda})_2]^n$ with $n = 0$ for **1** and $n = 2-$ for **2**. The anion $n = 1-$ has been reported previously in the coordination salt $[\text{Fe}(\text{dad})_3][\text{Fe}(\text{pda})_2]$ (**3**; $\text{dad} = N,N'$ -bis-

(phenyl)-2,3-dimethyl-1,4-diaza-1,3-butadiene). A complicated temperature-dependent electronic structure has been observed for this salt. Here, DFT calculations performed on **3** confirm the previous assignments of spin- and oxidation-states. Thus, $[\text{Fe}(\text{pda})_2]^n$ ($n = 0, 1-, 2-$) constitutes an electron-transfer series, which has also been established by cyclic voltammetry; the mono- and dications ($n = 1+$ and $2+$) are also accessible in solution, but have not been further investigated. The ^{57}Fe Mössbauer spectra of $[\text{Fe}(\text{pda})_2]^n$ species in **1** and **3** show extremely large quadrupole splitting constants due to addition of the valence and covalence contributions that have been confirmed by DFT calculations.

Keywords: density functional calculations • iron • Moessbauer spectroscopy • non-innocent ligands • redox chemistry

Introduction

The coordination chemistry of metal complexes with redox-active (non-innocent) ligands is presently undergoing a renaissance due to the recognition that redox processes in some enzymes and their model compounds may involve not only metal centers, but also coordinated ligands.^[1] Redox-active ligands in complexes can play not only their conventional role as ancillary units, but also they may be involved in redox events. This has opened new aspects in synthetic chemistry and catalysis.^[2] Moreover, the potential broad application of such complexes in material science as memory devices, molecular switches, and molecular magnets have been suggested.^[3] With this in mind our current research is dedicated to development of the deeper understanding of

[a] Dr. M. M. Khusniyarov, Dr. E. Bill, Dr. T. Weyhermüller, Dr. E. Bothe, Prof. Dr. K. Wieghardt
Max-Planck-Institut für Bioorganische Chemie
Stiftstrasse 34–36, 45470 Mülheim an der Ruhr (Germany)
Fax: (+49) 208-306-3951
E-mail: marik@mpi-muelheim.mpg.de
wieghardt@mpi-muelheim.mpg.de

[b] Dr. M. M. Khusniyarov, Dr. K. Harms, Prof. Dr. J. Sundermeyer
Fachbereich Chemie, Philipps-Universität Marburg
Hans-Meerwein-Straße, 35032 Marburg (Germany)
Fax: (+49) 6421-28-28917
E-mail: jsu@chemie.uni-marburg.de

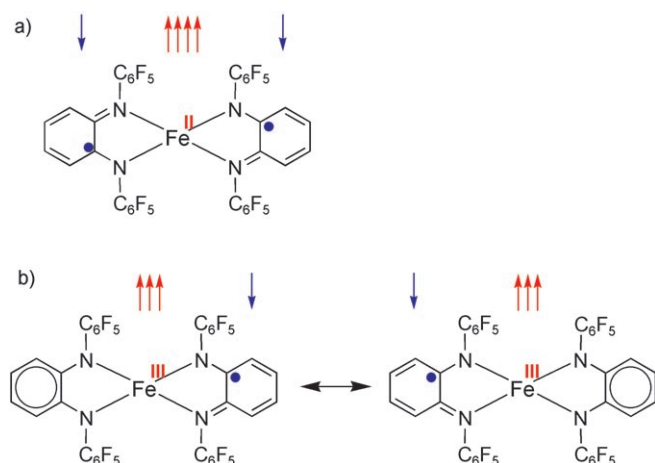
Supporting information for this article is available on the WWW under <http://dx.doi.org/10.1002/chem.200800546>.

the electronic structures of coordination compounds featuring redox-active ligands.^[4]

Very recently we reported on a series of four-coordinate, tetrahedral iron complexes $[\text{Fe}(\text{dad})_2]^0$ containing two chelating 1,4-diaza-1,3-butadiene substituted ligands (dad).^[5] By using a range of spectroscopic methods, low-temperature X-ray crystallography, and DFT calculations it was unambiguously shown that the correct description of these complexes, possessing a triplet ground state, is $[\text{Fe}^{\text{II}}(\text{dad}^-)_2]$, that is, a high-spin Fe^{II} ion (d^6 , $S_{\text{Fe}}=2$) coupled antiferromagnetically to two $\text{dad}^{\cdot-}$ π -radical anionic ligands.^[5]

Information about the corresponding *o*-phenylenediamido (*pda*) complexes is scarce, and only one dimeric homoleptic complex, $[[\text{Fe}(\text{pda})_2]_2]^0$, has been reported so far.^[6] It was proposed^[6] that this complex is composed of two nearly square-planar $[\text{Fe}(\text{pda})_2]^0$ fragments combined into a diamagnetic dimer so that the iron centers achieve FeN_5 square-pyramidal geometry. Monomeric $[\text{Fe}(\text{pda})_2]^0$ complexes have not been isolated to date.

Here we report the monomeric complex $[\text{Fe}(\text{pda})_2]$ (**1**), in which *pda* is an *N,N'*-bis(pentafluorophenyl)-*o*-phenylenediamido ligand (Scheme 1). Similar to the reported $[\text{Fe}$

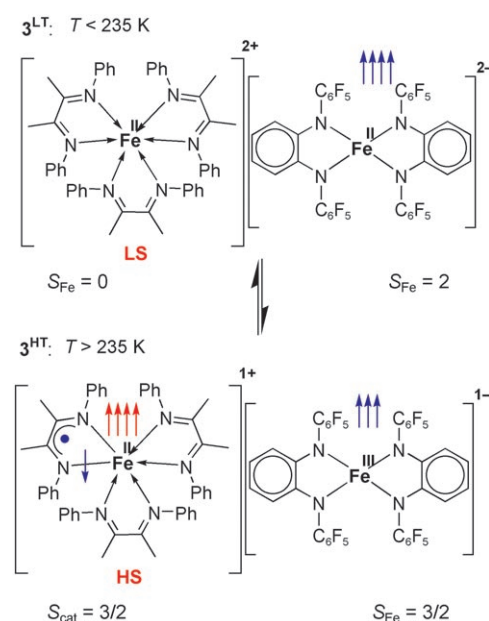


Scheme 1. Two alternative descriptions for the electronic structure of **1** ($S_1=1$) comprising C_6F_5 substituents: a) a ferrous complex $[\text{Fe}^{\text{II}}(\text{pda}^-)_2]^0$ or b) a ferric species $[\text{Fe}^{\text{III}}(\text{pda}^{2-})(\text{pda}^-)]^0$.

$(\text{dad})_2]$ complexes, **1** possesses a distorted tetrahedral geometry and a triplet ground state; however, the electronic structure of **1** turns out to be completely different. On the basis of the presented experimental and theoretical studies **1** must be described as $[\text{Fe}^{\text{III}}(\text{pda}^{2-})(\text{pda}^-)]^0$ containing an intermediate-spin Fe^{III} ion (d^5 , $S_{\text{Fe}}=3/2$) coupled antiferromagnetically to one ligand π -radical $\text{pda}^{\cdot-}$ ion. Thus **1** is a very rare example^[7] of an intermediate-spin ferric ion in a truly four-coordinate environment. To prove this assignment of oxidation and spin states in **1**, we also prepared and thor-

oughly characterized its doubly reduced counterpart $[\text{AsPh}_4][\text{Fe}^{\text{II}}(\text{pda}^{2-})_2]$ **2**, which possesses a central high-spin Fe^{II} ion. Although the redox series $[\text{M}(\text{pda})_2]^{2-/-1-/0/1+/2+}$ ($\text{M}=\text{Ni}, \text{Pd}, \text{Pt}$) have been established since the pioneering work of Balch and Holm in 1966,^[8] this is the first time that such a dianionic species has been isolated and structurally characterized.

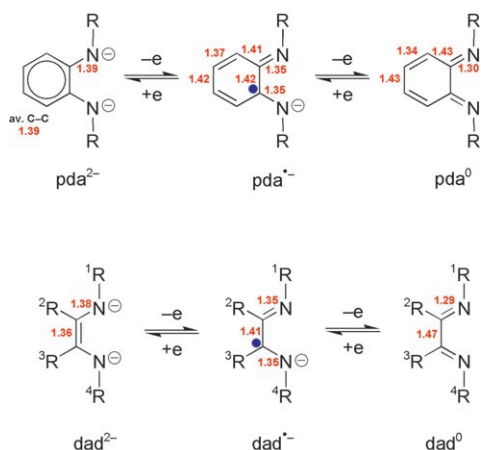
We recently reported the synthesis, X-ray structure determination, and spectroscopic investigation of the coordination salt $[\text{Fe}(\text{dad})_3][\text{Fe}(\text{pda})_2]$ (**3**; $\text{dad} = N,N'$ -bis(phenyl)-2,3-dimethyl-1,4-diaza-1,3-butadiene).^[9] This salt possesses a complicated temperature-dependent electronic structure (Scheme 2). At low temperature, **3**^{LT} contains: 1) a diamag-



Scheme 2. Temperature-dependent electronic structure of $[\text{Fe}(\text{dad})_3][\text{Fe}(\text{pda})_2]$ **3**: **3**^{LT} below 235 K and **3**^{HT} above 235 K.

netic octahedral dication containing a low-spin Fe^{II} ion and three neutral dad^0 ligands, and 2) a paramagnetic distorted tetrahedral dianion consisting of a high-spin Fe^{II} center with two closed-shell dianionic ligands pda^{2-} as in **2**. At high temperature, **3**^{HT} is composed of: 1) an octahedral monocation with a high-spin Fe^{II} ion, two neutral dad^0 ligands and one π -ligand radical $\text{dad}^{\cdot-}$, 2) a monoanion containing an intermediate-spin Fe^{III} central ion with two closed-shell dianionic pda^{2-} ligands. Thus, **3** shows reversible, thermally induced, electron transfer within a cation–anion pair coupled to spin crossover.^[9] In this study we present additional spectroscopic data and DFT calculations for both **3**^{LT} and **3**^{HT}.

It is established that the three oxidation levels of the ligands $\text{dad}^{2-/-1-/0}$ and $\text{pda}^{2-/-1-/0}$ can be clearly distinguished in coordination compounds by cryogenic X-ray crystallography.^[48] As shown in Scheme 3 the C–N bond lengths vary in a characteristic fashion: in the closed-shell dianions dad^{2-} and pda^{2-} they are relatively long at $1.38 \pm 0.01 \text{ \AA}$; they shrink to $1.35 \pm 0.01 \text{ \AA}$ in the π -radical monoanions $\text{dad}^{\cdot-}$



Scheme 3. Different redox states of *o*-phenylenediamide (pda) and 1,4-diaza-1,3-butadiene (dad) derived ligands.

and pda^{•-}; and they are short double bonds at 1.29 ± 0.01 Å in the closed-shell neutral ligands dad⁰ and pda⁰. Similarly, the C_{imine}-C_{imine} bonds vary from 1.36 ± 0.01 Å in the dianion to 1.41 ± 0.01 Å in the monoanionic π radical, to 1.47 ± 0.01 Å in the neutral dad⁰ ligand. The six-membered phenyl ring in pda²⁻ displays six nearly equivalent aromatic C-C bonds at ≈ 1.40 Å, whereas the same ring in neutral pda⁰ exhibits a marked quinoid distortion, which is slightly less pronounced in the π -radical monoanion pda^{•-}. Intermediate C-N and C-C bonds lengths may be expected in complexes with one pda^{•-} radical and a dianion if the unpaired electron is delocalized; but these cases are usually beyond the resolution and accuracy of single-crystal X-ray crystallography.

Results and Discussion

Crystal structures: The molecular structure of **1** consists of two chelating pda ligands bound to an iron center. The complex has a twisted geometry intermediate between planar and tetrahedral with a twist angle of 54.0° (Figure 1). This geometry results from intramolecular π - π interactions between two pairs of C₆F₅ rings.^[10,11] Each C₆F₅ ring is not orthogonal to the corresponding ligand backbone C₆H₄N₂Fe, but is inclined so as to form a dihedral angle in the range 49.9 – 54.8° . Interestingly, although **1** contains two identical and symmetrical ligands, the complex is chiral. A helix-like structure results from the two C₆F₅/C₆F₅ pairs in the *cis*-position of the molecule, at which the two rings are parallel to each other in pairs, but the two pairs are turned relative to the ligand backbones in the opposite directions (Figure 2). The source of this chirality is the rotational barrier of each of the C₆F₅ rings around the C-N bond that is introduced by its intramolecular proximity to a second C₆F₅ group.

The local symmetry at the iron center approximates to *D*₂, the two *N,N*-coordinated pda ligands have very similar geometric parameters. Bond lengths within each of the ligand backbones reveal a weak quinoid-type distortion: C-N (av $1.382(4)$ Å) and short conjugated C-C (av

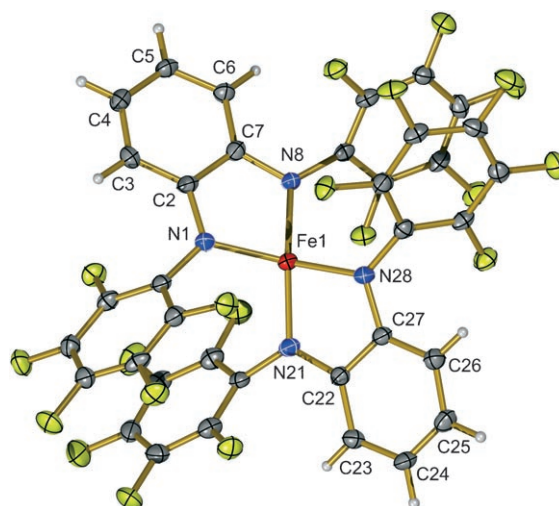


Figure 1. Molecular structure of **1**, thermal ellipsoids are drawn at the 60% probability level.

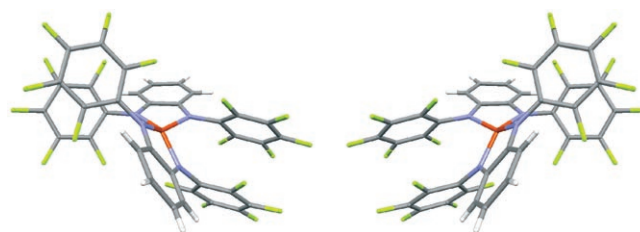


Figure 2. Two enantiomers of the [Fe(pda)₂]ⁿ fragment in complexes **1–3** (*n*=0, 1–, 2–).

$1.373(4)$ Å) bonds, and long residual C-C bonds (av $1.410(4)$ Å) (Table 1). This geometric pattern resembles that found for the series of complexes [M^{II}(pda^{•-})₂] (M = Co, Ni, Pd, Cu), all of which contain a pair of π -radical ligands coordinated to a divalent metal ion.^[10] Thus, the electronic structure of **1** could be described as [Fe^{II}(pda^{•-})₂], that is, a ferrous complex containing two radical ligands. Since the short Fe-N bond lengths (av $1.897(3)$ Å) rule out the high-spin ferrous ion, [Fe^{II}(pda^{•-})₂] should have an intermediate-spin ferrous center (*S*_{Fe}=1), which is expected to couple antiferromagnetically to two radical ligands (*S*_R=1) giving a diamagnetic complex (*S*_t=0). However, it is in contradiction with the fact that the complex is paramagnetic with a ground state triplet (*vide infra*).

The other possibility to describe the electronic structure of **1** is [Fe^{III}(pda²⁻)(pda^{•-})]—an intermediate-spin ferric ion (*S*_{Fe}=3/2) coordinated by one radical pda^{•-} ligand (*S*_R=1/2) and one closed-shell dianion pda²⁻. The observed close similarity in the bond parameters of the two pda ligands would then require a delocalized Class II or Class III mixed valence system. In this case the bond lengths within pda backbones in **1** should be the arithmetical average between those in pda²⁻ and the radical pda^{•-}. Indeed, the quinoid-type distortion in **1** is less pronounced compared to the series of [M^{II}(pda^{•-})₂] (M = Co, Ni, Pd, Cu) complexes.^[10] Since the structure of **1** has $3\sigma_{C-C}$ of 0.012 Å, we cannot distinguish

Table 1. Selected bond lengths [\AA] and a twist angle [$^\circ$] of **1**, **2**, and $[\text{Fe}^{\text{II}}(\text{pda}^{2-})_2]^{2-}$ from **3^{LT}**.

	1	2	3^{LT} ^[a]
Fe1–N1	1.895(3)	2.030(5)	2.004(2)
Fe1–N8	1.900(2)	2.039(4)	1.988(2)
Fe1–N21	1.902(2)		
Fe1–N28	1.892(3)		
C2–N1	1.380(4)	1.411(7)	1.401(3)
C7–N8	1.379(4)	1.389(7)	1.396(4)
C22–N21	1.381(4)		
C27–N28	1.387(4)		
C3–C4	1.367(4)	1.391(8)	1.394(4)
C5–C6	1.373(4)	1.390(8)	1.394(4)
C23–C24	1.375(4)		
C25–C26	1.377(4)		
C4–C5	1.406(4)	1.392(8)	1.364(4)
C2–C7	1.426(4)	1.428(8)	1.428(4)
C2–C3	1.404(4)	1.383(8)	1.392(4)
C6–C7	1.402(4)	1.405(8)	1.390(4)
C24–C25	1.405(5)		
C22–C27	1.422(4)		
C22–C23	1.412(4)		
C26–C27	1.401(4)		
α ^[b]	54.0	44.9	57.1

[a] Taken from reference [9]. [b] The dihedral angle between the two $\text{C}_6\text{H}_4\text{N}_2\text{Fe}$ planes.

between $[\text{Fe}^{\text{II}}(\text{pda}^-)_2]$ and $[\text{Fe}^{\text{III}}(\text{pda}^{2-})(\text{pda}^-)]$ with sufficient confidence relying on X-ray studies.

The molecular structure of **2** consists of a $[\text{Fe}(\text{pda})_2]^{2-}$ dianion (Figure 3) and two $[\text{AsPh}_4]^+$ counterions. The twisted geometry of the dianion resembles that of the neutral complex **1**. The twist angle of 44.9° in **2** is slightly smaller than that in **1**; however, the intramolecular π – π stacking motif is preserved and the interplanar $\text{C}_6\text{F}_5/\text{C}_6\text{F}_5$ distances in **1** and **2** are very similar. A crystallographically imposed C_2 axis renders the two pda ligands identical. In contrast to **1**, no quinoid-type distortion is observed in **2**; the two phenylene rings are aromatic (av C–C 1.398(8) \AA), and the long C–N

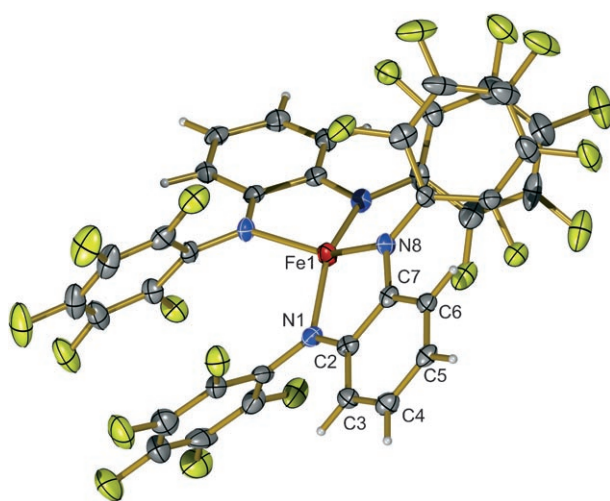


Figure 3. Molecular structure of the dianion (site symmetry C_2) in **2**, thermal ellipsoids are drawn at the 40% probability level.

distances correspond to single bonds (av 1.400(7) \AA), consistent with the presence of two closed-shell pda^{2-} ligands. Consequently, the electronic structure of the dianion in **2** is $[\text{Fe}^{\text{II}}(\text{pda}^{2-})_2]^{2-}$ —two closed-shell pda^{2-} ligands bound to a ferrous ion. The four long Fe–N bonds (av 2.035(5) \AA) in a highly distorted tetrahedral geometry indicate a high-spin state of Fe^{II} . Very recently we reported on the low-temperature crystallographical characterization of the same dianion in a coordination salt $[\text{Fe}^{\text{II}}(\text{dad}^0)_3]^{2+}[\text{Fe}^{\text{II}}(\text{pda}^{2-})_2]^{2-}$ **3^{LT}**,^[9] for which selected geometrical parameters are given in Table 1.

Although several dianions $[\text{M}(\text{pda}^{2-})_2]^{2-}$ ($\text{M} = \text{Ni}, \text{Pd}, \text{Pt}$) that contain two fully reduced pda^{2-} ligands have been generated electrochemically and characterized by electronic spectroscopy in the past,^[12] these highly sensitive species have not been isolated and crystallographically characterized to date. Thus, $[\text{Fe}^{\text{II}}(\text{pda}^{2-})_2]^{2-}$ in **2** and **3^{LT}** is the first such example and its geometric details may serve as a reference point for the fully reduced ligand form of the *o*-phenylenediamide ligand.^[13] Surprisingly, the geometry of $[\text{Fe}^{\text{II}}(\text{pda}^{2-})_2]^{2-}$ in **2** and **3^{LT}** is similar, but not identical. The dianion in **2** has a 12° less twisted geometry compared to **3^{LT}**, which we ascribed to differing packing forces in the unit cell.

Magnetism: The results of temperature-dependent magnetic susceptibility measurements on paramagnetic **1** and **2** are shown in Figures 4 and 5, respectively. The observed effective

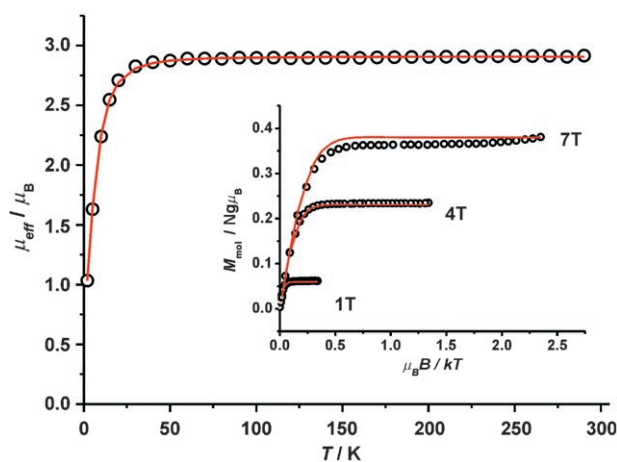


Figure 4. Temperature dependence of the effective magnetic moment of **1** recorded at 1 T. The inset shows multiple-field temperature dependence of the magnetization of **1**. The solid lines in red represent the best fit obtained with $g_i = 2.06$, $D_i = 22.4 \text{ cm}^{-1}$, $E/D_i = 0.0$.

ive magnetic moment (μ_{eff}) of $2.90 \mu_{\text{B}}$ for **1** is nearly temperature independent in the range 60–290 K, consistent with a ground state triplet ($S_i = 1$), which is the only thermally populated state at temperatures up to 290 K. The decrease of μ_{eff} below 60 K is due to zero-field splitting ($D_i = +22.4 \text{ cm}^{-1}$, $E/D_i = 0.0$). A ground-state triplet can be obtained either by a strong antiferromagnetic (AF) coupling of a high-spin Fe^{II} ($S_{\text{Fe}} = 2$) with two radical ligands as in $[\text{Fe}^{\text{II}}(\text{pda}^-)_2]$, or by a strong AF coupling of one radical ligand

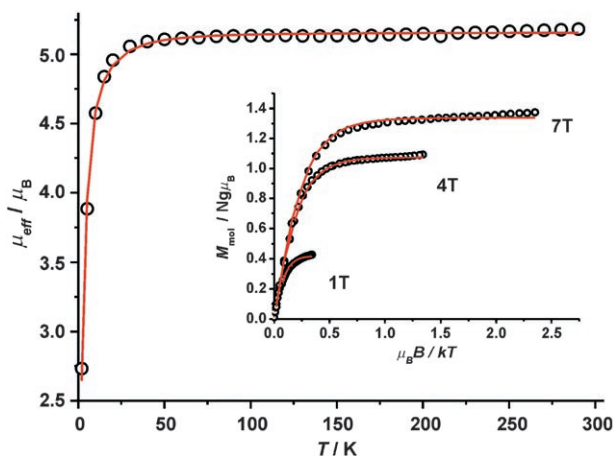


Figure 5. Temperature dependence of the effective magnetic moment of **2** recorded at 1 T. The inset shows multiple-field temperature dependence of the magnetization of **2**. The solid lines in red represent the best fit obtained with $g=2.11$, $D=12\text{ cm}^{-1}$, $E/D=0.17$.

with an intermediate-spin Fe^{III} ($S_{\text{Fe}}=3/2$) as in $[\text{Fe}^{\text{III}}(\text{pda}^-)(\text{pda}^{2-})]$ (Scheme 1).

In the case of **2**, the effective magnetic moment $\mu_{\text{eff}}=5.15\mu_{\text{B}}$ is temperature independent in the temperature range 60–290 K corresponding to a ground-state quintet ($S_{\text{Fe}}=2$). Zero-field splitting of the $S_{\text{Fe}}=2$ state ($D=+12\text{ cm}^{-1}$, $E/D=0.17$) affects the magnetic moment at temperatures $T < 60\text{ K}$. The results of these SQUID measurements combined with X-ray crystallographic studies suggest that the electronic structure of the dianion in **2** must be described as $[\text{Fe}^{\text{II}}(\text{pda}^{2-})_2]^{2-}$, containing a high-spin Fe^{II} center and two closed-shell dianionic ligands.

Mössbauer spectroscopy: The zero-field ^{57}Fe Mössbauer spectra of **1** and **2** at 80 K are shown in Figures 6 and 7, respectively. The spectrum of **1** reveals a quadrupole doublet with a low isomer shift $\delta=0.23\text{ mm s}^{-1}$ and a very large quadrupole splitting $|\Delta E_{\text{Q}}|=4.45\text{ mm s}^{-1}$. It is worthwhile to compare the Mössbauer parameters of **1** with those of the closely related series of $[\text{Fe}^{\text{II}}(\text{dad}^-)_2]$ complexes,^[5] in which dad^- is a set of π -radical ligands derived from differently substituted 1,4-diaza-1,3-butadiene. These complexes possess

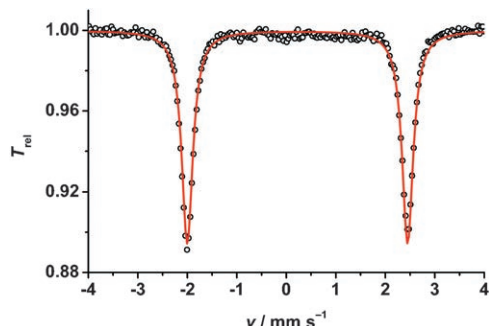


Figure 6. Zero-field ^{57}Fe Mössbauer spectrum of crystalline **1** recorded at 80 K, the solid line represents the best fit obtained with parameters: $\delta=0.23\text{ mm s}^{-1}$, $|\Delta E_{\text{Q}}|=4.45\text{ mm s}^{-1}$.

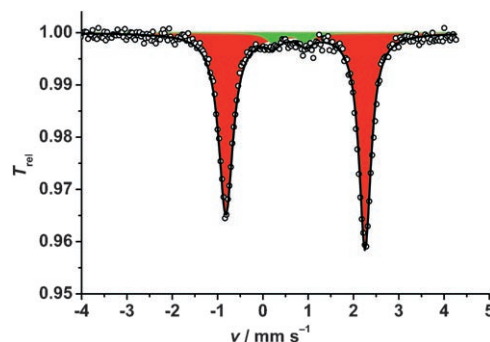


Figure 7. Zero-field ^{57}Fe Mössbauer spectrum of crystalline **2** recorded at 80 K, the solid line represents the best fit obtained with parameters: a) **2**, $\delta=0.72\text{ mm s}^{-1}$, $|\Delta E_{\text{Q}}|=3.07\text{ mm s}^{-1}$; b) an unidentified impurity, $\delta=0.59\text{ mm s}^{-1}$, $|\Delta E_{\text{Q}}|=0.72\text{ mm s}^{-1}$. Color scheme: **2** in red, the impurity (<5%) in green.

a nearly tetrahedral or twisted geometry and contain a high-spin Fe^{II} center. The comparatively high isomer shifts for $[\text{Fe}^{\text{II}}(\text{dad}^-)_2]$ complexes observed in the range 0.50–0.65 mm s^{-1} are in stark contrast to the much lower isomer shift of **1**, which renders the description of **1** as $[\text{Fe}^{\text{II}}(\text{pda}^-)_2]$, that is, as a high-spin Fe^{II} complex, highly unlikely. On the other hand, the Mössbauer parameters of **1** closely resemble those of an intermediate-spin ferric ion in square-pyramidal complexes.^[6,14] Thus, the correct description of the electronic structure of **1** must be $[\text{Fe}^{\text{III}}(\text{pda}^-)(\text{pda}^{2-})]$, that is, an intermediate-spin Fe^{III} ($S_{\text{Fe}}=3/2$) with one mono-anionic π -radical pda^- ligand and one closed-shell pda^{2-} ion. Indeed, the Mössbauer parameters of **1** are very similar to the values reported for the intermediate-spin Fe^{III} anion $[\text{Fe}^{\text{III}}(\text{pda}^{2-})_2]^-$ in **3^{HT}** (HT=refers to the high-temperature form; $S=3/2$) ($\delta=0.16$ and $|\Delta E_{\text{Q}}|=4.19\text{ mm s}^{-1}$).^[9]

A frozen solution of ^{57}Fe -enriched **1** ($c \approx 5\text{ mM}$, in toluene) was used for applied-field Mössbauer spectroscopy. Five spectra, acquired at different low temperatures and different applied fields, with fit parameters are shown in Figure 8. During the fitting procedure the three components of the \mathbf{g} tensor and the zero-field splitting (ZFS) parameters were fixed as determined from the magnetic-susceptibility measurements. The quadrupole splitting is very large and positive, and the asymmetry parameter $\eta=0.64$. Interestingly, although the electric-field gradient (EFG) and the hyperfine coupling tensors have common principle axes, the EFG tensor is rotated by 90° relative to the hyperfine coupling tensor \mathbf{A} (Figure S1 in the Supporting Information).

The zero-field Mössbauer spectrum of **2** shows a major species (>95%) with a high isomer shift $\delta=0.72\text{ mm s}^{-1}$ and a large quadrupole splitting $|\Delta E_{\text{Q}}|=3.07\text{ mm s}^{-1}$, which points unambiguously to a high-spin Fe^{II} center. A crystalline sample of **2** was used for applied-field measurements (Figure 9). The best fit was obtained with an asymmetry parameter $\eta=1.0$, which requires two nearly identical major components of the EFG tensor with opposite signs and the third component close to zero, which renders the sign of the quadrupole splitting parameter physically meaningless.

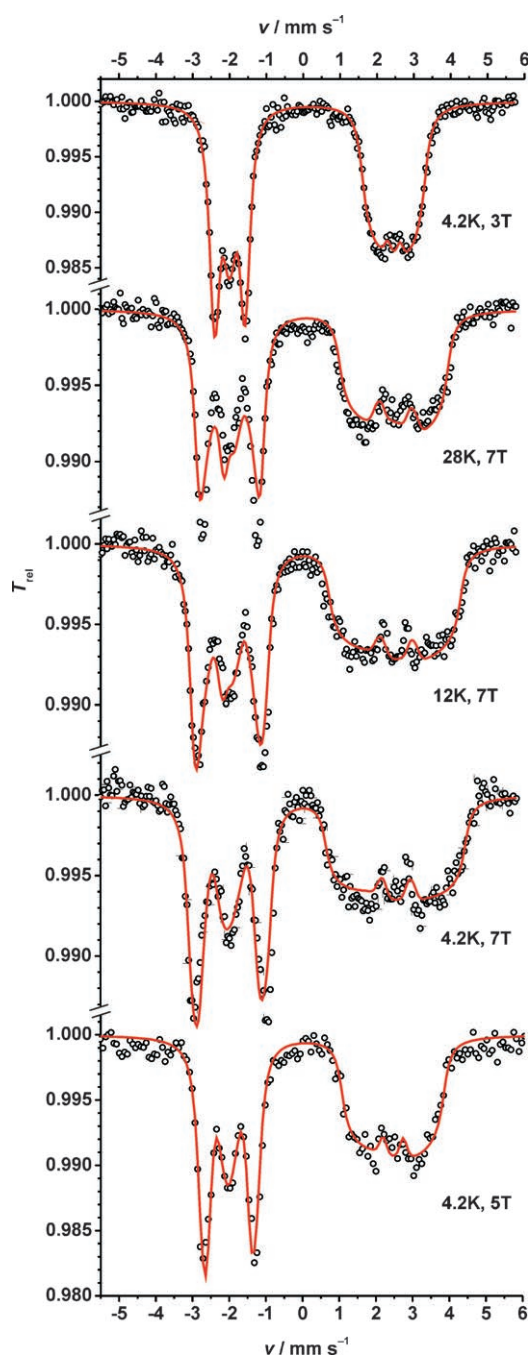


Figure 8. Applied-field ^{57}Fe Mössbauer spectra of frozen toluene solutions of ^{57}Fe enriched **1** recorded at different low temperatures and different applied fields. The solid lines in red represent the best fit obtained with parameters: $S_{\text{Fe}}=1$, $\delta=0.23\text{ mm s}^{-1}$, $\Delta E_{\text{O}}=+4.44\text{ mm s}^{-1}$, $\eta=0.64$; $D_{\text{I}}=+22\text{ cm}^{-1}$, $E/D_{\text{I}}=0.0$; $g_x=g_y=g_z=2.06$, $A_{\text{I},xx}=9.9$, $A_{\text{I},yy}=-21.9$, $A_{\text{I},zz}=10.6\text{ T}$, $\beta=90^\circ$.^[47] The effective (total) \mathbf{D} and \mathbf{A} tensors obtained for the ground triplet can be converted into the local tensors using the spin projection techniques: $D_{\text{Fe}}=2/3D_{\text{I}}=14.7\text{ cm}^{-1}$; $A_{\text{Fe},xx}=4/5 A_{\text{I},xx}=7.9$, $A_{\text{Fe},yy}=-17.5$, $A_{\text{Fe},zz}=8.5\text{ T}$.

Surprisingly, in spite of the fact that **2** and **3^{LT}** contain the same dianion, $[\text{Fe}^{\text{II}}(\text{pda}^{2-})_2]^{2-}$, the zero-field Mössbauer spectra of their polycrystalline samples are not identical. While the isomer shifts for the anions are very similar (0.72

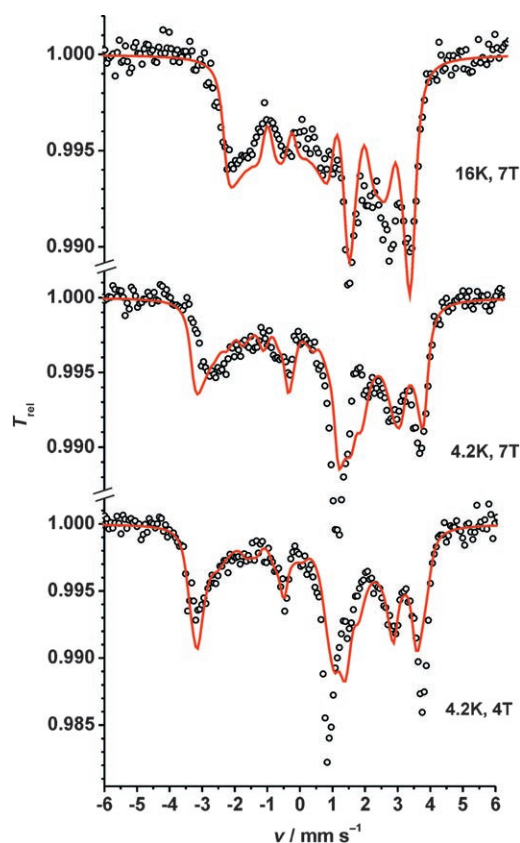


Figure 9. Applied-field ^{57}Fe Mössbauer spectra of crystalline **2** recorded at different low temperatures and different applied fields. The solid lines in red represent the best fit obtained with parameters: $S_{\text{Fe}}=2$; $\delta=0.72\text{ mm s}^{-1}$, $\Delta E_{\text{O}}=+2.93\text{ mm s}^{-1}$, $\eta=1.0$; $D=+12\text{ cm}^{-1}$, $E/D=0.17$; $g_x=g_y=g_z=2.11$, $A_{xx}=-2.0$, $A_{yy}=-12.1$, $A_{zz}=-2.0\text{ T}$, $\beta=31^\circ$. The slight deviations of the actual fit from the experimental data are supposed to be due to intermolecular interactions in solid **2** and probably due to a texture effect.

and 0.68 mm s^{-1} , respectively), the quadrupole splitting constants are very different: large for **2** (3.07 mm s^{-1}) and extraordinarily large for **3^{LT}** (5.20 mm s^{-1}). This effect may arise from the different twist angles shown by the X-ray studies ($\alpha=44.8^\circ$ in **2** and $\alpha=57.1^\circ$ in **3^{LT}**). It is surprising that such a minor change in geometry induces such a large influence on the EFG.

The zero-field Mössbauer spectra of **3^{LT}** and **3^{HT}** have been reported.^[9] Here, a successful simulation of the applied-field Mössbauer spectra obtained for crystalline **3^{LT}** is presented (Figure 10). Each spectrum obtained at different field and temperature can be deconvoluted into the two sub-spectra of the same intensity with $\delta=0.37\text{ mm s}^{-1}$, $\Delta E_{\text{O}}=-0.54\text{ mm s}^{-1}$ assigned to the low-spin Fe^{II} in an octahedral dication, $[\text{Fe}^{\text{II}}(\text{dad}^0)_3]^{2+}$, and $\delta=0.68\text{ mm s}^{-1}$, $\Delta E_{\text{O}}=-5.20\text{ mm s}^{-1}$ assigned to the high-spin Fe^{II} in the twisted tetrahedral $[\text{Fe}^{\text{II}}(\text{pda}^{2-})_2]^{2-}$ ion. The dication is clearly diamagnetic showing only the nuclear Zeeman splitting induced by the applied field; the negative sign of the quadrupole splitting parameter agrees well with similar dications.^[15] The dianion shows the presence of a strong internal magnetic

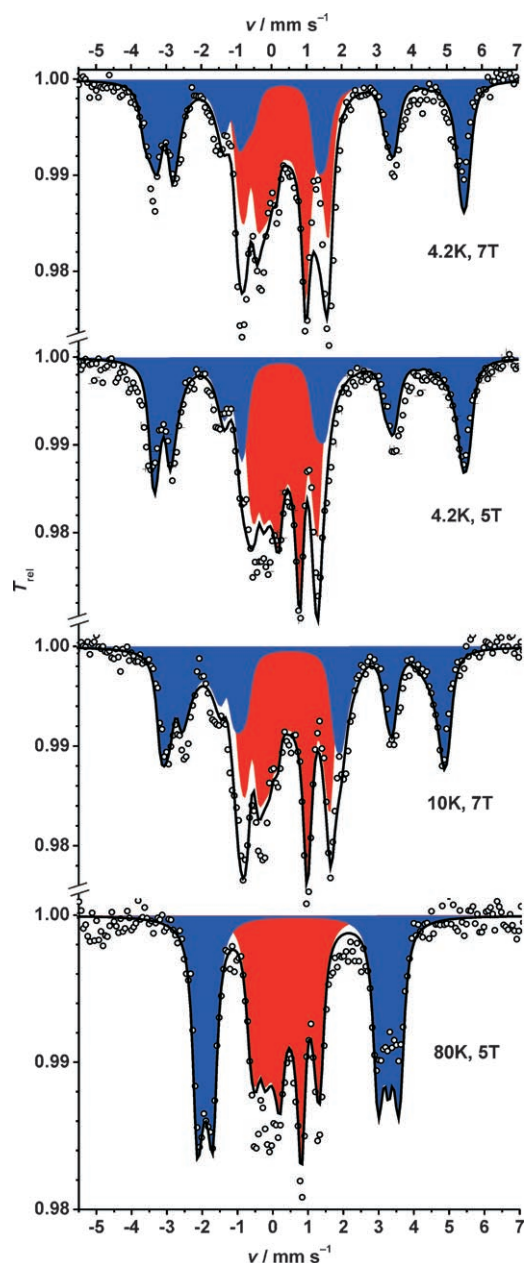


Figure 10. Applied-field ^{57}Fe Mössbauer spectra of crystalline 3^{LT} recorded at different low temperatures and different applied fields. The solid lines represent the best fit obtained with parameters: a) diamagnetic dication, $S_{\text{Fe}}=0$, $\delta=0.37\text{ mm s}^{-1}$, $\Delta E_{\text{O}}=-0.54\text{ mm s}^{-1}$, $\eta=0.0$; b) paramagnetic dianion, $S_{\text{Fe}}=2$, $\delta=0.68\text{ mm s}^{-1}$, $\Delta E_{\text{O}}=-5.20\text{ mm s}^{-1}$, $\eta=0.3$, $D=+5\text{ cm}^{-1}$, $E/D=0.0$, $g_x=g_y=g_z=2.00$, $A_{xx}=-12.5$, $A_{yy}=-12.5$, $A_{zz}=-23.0\text{ T}$. Color scheme: dianion in blue, dication in red.

field; the sign of the quadrupole splitting parameter is negative and the asymmetry parameter η is 0.3. Note that all three components of the hyperfine coupling tensor for both dianions $[\text{Fe}^{\text{II}}(\text{pda}^{2-})_2]^{2-}$ in 2 and 3^{LT} are negative.

Electronic spectra: The electronic spectra of 1 and 2 measured in the range 250–2000 nm are very different (Figure 11). The UV/Vis/NIR spectrum of 1 is dominated by a series of intense CT bands in the visible region and one in-

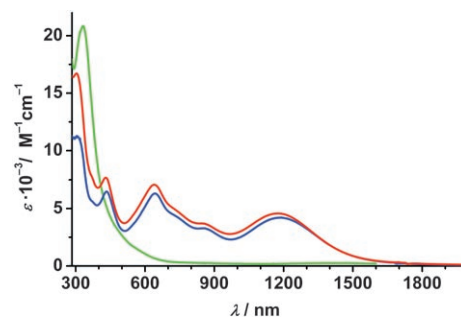


Figure 11. Electronic spectra of 1 measured in DME (red) and toluene (blue), and of 2 measured in MeCN (green).

tense band in the NIR ($\nu_{\text{max}}=1190\text{ nm}$, $\epsilon=4.2 \times 10^3\text{ M}^{-1}\text{ cm}^{-1}$). This intense band is assigned to a ligand-to-ligand intervalence charge-transfer (LLIVCT) band for mixed-valent $[\text{Fe}^{\text{III}}(\text{pda}^{\cdot-})(\text{pda}^{2-})]$. Since the experimental half-width of the LLIVCT band $\Delta\nu_{\text{exptl}}=2270\text{ cm}^{-1}$ is significantly smaller than a half-width calculated at $\Delta\nu_{\text{calcd}}=4410\text{ cm}^{-1}$ by using the Hush equation,^[16] $[\text{Fe}^{\text{III}}(\text{pda}^{\cdot-})(\text{pda}^{2-})]$ is assigned to a fully delocalized Class III system. The electronic spectra of 1 measured in dimethoxyethane or toluene are identical, whereas the spectrum recorded in acetonitrile changed significantly (Figure S2 in the Supporting Information). This can be ascribed to changes in the geometry of the complex due to coordination of acetonitrile. In contrast to 1 , complex 2 shows only one very intense band in the UV region (331 nm , $\epsilon=2.1 \times 10^4\text{ M}^{-1}\text{ cm}^{-1}$), which confirms the absence of ligand radicals in 2 .

Cyclic voltammetry: The cyclic voltammogram of 1 in acetonitrile at 20°C (glassy carbon working electrode, 200 mV s^{-1} scan rate, 0.10 M $[\text{nBu}_4\text{N}]\text{PF}_6$ as supporting electrolyte) is shown in Figure 12. Four reversible one-electron transfer waves are observed in the range 0.5 to -2.0 V versus Fc^+/Fc (ferrocenium/ferrocene), two of which at $E_{1/2}^1=0.063\text{ V}$ and $E_{1/2}^2=0.386\text{ V}$ correspond to oxidations, whereas $E_{1/2}^3$ at -0.337 V and $E_{1/2}^4=-1.351\text{ V}$ vs. Fc^+/Fc correspond to two successive reductions.

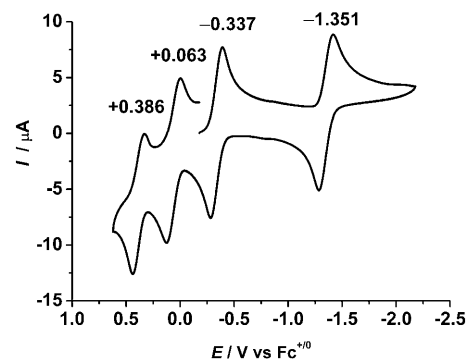
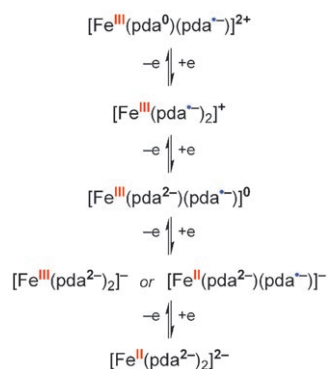


Figure 12. Cyclic voltammogram of 1 measured in MeCN at room temperature (glassy carbon working electrode, 200 mV s^{-1} scan rate, 0.10 M $[\text{nBu}_4\text{N}]\text{PF}_6$); the numbers on the graph are half-wave potentials, $E_{1/2}$.



The doubly reduced form $[\text{Fe}^{\text{II}}(\text{pda}^{2-})_2]^{2-}$ corresponds to the dianion in **2**, whereas the monoanion is either $[\text{Fe}^{\text{III}}(\text{pda}^{2-})_2]^{1-}$ or $[\text{Fe}^{\text{II}}(\text{pda}^{2-})(\text{pda}^-)]^{1-}$ as in the low- and high-temperature form of the salt $[\text{Fe}(\text{dad})_3][\text{Fe}(\text{pda})_2]$.^[9] The two oxidation processes for **1** are presumably ligand based. All redox potentials for **1** are strongly shifted to more positive voltages relative to other known $[\text{M}(\text{pda})_2]$ complexes.^[8,12,17] The presence of four strongly electron-withdrawing C_6F_5 groups destabilizes the oxidized, but stabilizes the reduced species. It is this fact that ultimately allowed us to isolate and crystallographically characterize the doubly reduced $[\text{Fe}^{\text{II}}(\text{pda}^{2-})_2]^{2-}$ species in **2**.

Density function theory (DFT) calculations of 1 and 2: The geometry of **1** was optimized by using BP86,^[18,19] PW91,^[20] hybrid B3P86,^[18] and B3LYP^[21] density functionals. The B3LYP functional failed to reproduce the intramolecular π - π interactions between opposing C_6F_5 rings and consequently the twisted geometry, whereas the B3P86 functional significantly overestimated the Fe-N distances.^[22] Although satisfactory results were obtained with the BP86 and PW91 functionals, only the use of the B3LYP functional with empirical Van der Waals corrections (B3LYP + vdW) gave a geometry close to that found experimentally, in which the π - π interactions, the twist angle, the quinoid-type distortion and the Fe-N distance were all well reproduced (Table 2).

Attempts to find broken symmetry^[23,24] (BS) states BS-(3,1) and BS(4,2), and a conventional triplet state $M_S=1$ were undertaken. All calculations converged to the BS(3,1) solution. The high-spin state $M_S=2$, which was calculated based on the geometry optimized to the high-spin and BS

Table 2. Geometry optimization (bond lengths [Å] and twist angle [°]) of **1** and **2** with B3LYP + vdW.

	1		2	
	Calcd	Exptl ^[a]	Calcd	Exptl ^[a]
C2-C3	1.412	1.405(4)	1.404	1.394(8)
C3-C4	1.388	1.373(4)	1.404	1.391(8)
C4-C5	1.415	1.406(5)	1.398	1.392(8)
C2-C7	1.441	1.424(4)	1.444	1.428(8)
C2-N1	1.374	1.382(4)	1.391	1.400(7)
Fe1-N1	1.921	1.897(3)	2.028	2.035(5)
α ^[b]	48.0	54.0	54.9	44.9

[a] The average values are given. [b] The dihedral angle between the two $\text{C}_6\text{H}_4\text{N}_2\text{Fe}$ planes.

solutions, was higher in energy than the BS(3,1) state by 5.7–7.4 kcal mol⁻¹. The BS(3,1) solution corresponds to the electronic description of **1** as $[\text{Fe}^{\text{III}}(\text{pda}^-)(\text{pda}^{2-})]$, that is, an intermediate-spin Fe^{III} ion ($S_{\text{Fe}}=3/2$) coupled antiferromagnetically to one ligand radical ($S_{\text{R}}=1/2$) giving rise to a ground-state triplet ($S_{\text{T}}=1$). A doubly occupied $d_{x^2-y^2}$, singly occupied d_{xz} , d_{z^2} , and d_{yz} , and an unoccupied d_{xy} orbital represent an intermediate-spin Fe^{III} ion (Figure 13). One π -type ligand orbital found in the β set but not in the α set is a magnetic orbital of the ligand radical, which has an appropriate symmetry to couple antiferromagnetically with the magnetic iron d_{xz} orbital.

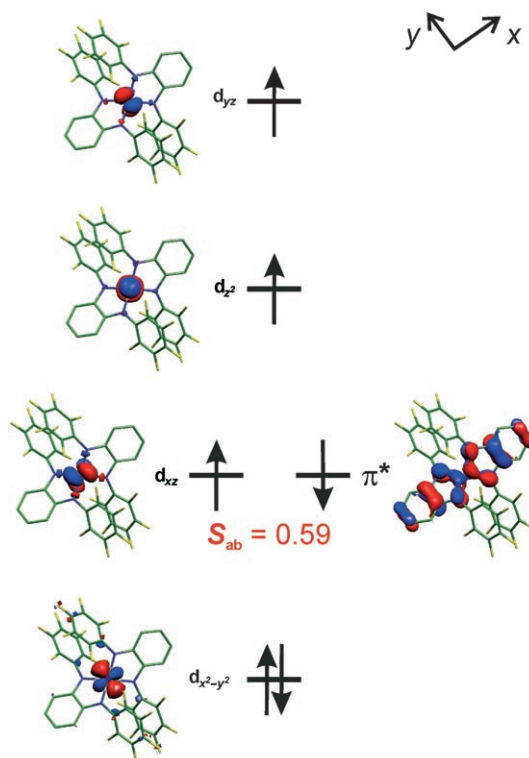


Figure 13. Qualitative MO Scheme for **1**; S_{ab} is an overlap integral for the pair of magnetic orbitals.

The calculated orbital overlap for two magnetic orbitals $S_{AB} = \langle \psi_A | \psi_B \rangle = 0.59$ shows substantial diradical character of this pair, in which $S_{AB}=1$ would represent a conventional bonding situation with corresponding α and β orbitals occupying the same space, and $S_{AB}=0$ would indicate orthogonal magnetic orbitals of a “pure” diradical.^[24,25] The large orbital overlap correlates with effective exchange coupling constant estimated by Equation (1),^[26] in which E_{HS} and E_{BS} are the total energies of the high-spin and BS state, respectively; $\langle S_{\text{HS}}^2 \rangle$ and $\langle S_{\text{BS}}^2 \rangle$ are the expectation values of the total spin-squared operator \hat{S}^2 for the high-spin and BS state, respectively; the Heisenberg operator $\hat{H} = -2J\mathbf{S}_A \cdot \mathbf{S}_B$ is valid here.

$$J = -\frac{E_{\text{HS}} - E_{\text{BS}}}{\langle S_{\text{HS}}^2 \rangle - \langle S_{\text{BS}}^2 \rangle} \quad (1)$$

Since the calculations give an effective exchange coupling constant $J = -640 \text{ cm}^{-1}$, the coupling is strong and antiferromagnetic. This is fully supported by SQUID measurements, in which the ground state triplet is the only thermally populated state at temperatures up to 290 K.

While the electronic configuration of the iron ion in $[\text{Fe}^{\text{III}}(\text{pda}^{\cdot-})(\text{pda}^{2-})]$ is shown in Table 3, the bonding situation can be nicely visualized by the BS spin density map^[27,28] (Figure 14). Positive spin density is mainly located at the

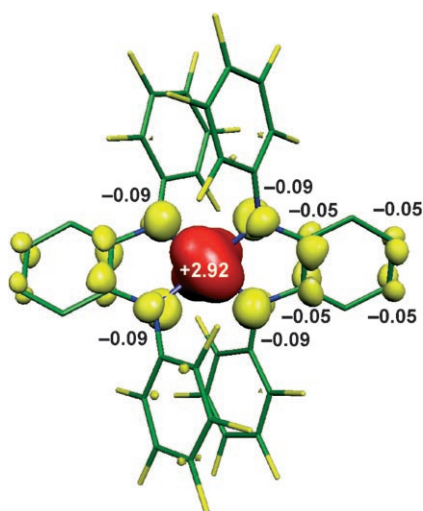


Figure 14. Broken symmetry spin density map for $[\text{Fe}^{\text{III}}(\text{pda}^{\cdot-})(\text{pda}^{2-})]$ in **1**.

iron center ($\rho_{\text{Fe}} = +2.92$), while negative spin density is symmetrically distributed over the both ligands ($\rho_{\text{L}} = -0.92$), suggestive of a delocalized mixed-valence system. The large quadrupole splitting and the low isomer shift of the Mössbauer doublet for **1** are very well reproduced by the calculations on the BS(3,1) state (Table 4). It is worth noting that in this work the Mössbauer parameters are calculated by using a calibration curve originally derived from the calculations of twenty-five various iron complexes optimized with the BP86 functional.^[29] It is surprising then that agreement between the calculated and the experimental Mössbauer parameters is better for **1** optimized with the B3LYP+vdw than the BP86 functional (see the Supporting Information).

Table 4. Calculation of properties for **1** and **2**.

	1	2
δ [mm s ⁻¹]	0.23 (0.23) ^[a]	0.63 (0.72)
ΔE_{O} [mms ⁻¹]	4.32 (4.45)	5.35 (3.07)
η	0.26 (0.64)	0.44 (1.0)
ρ_{Fe} ^[b]	2.92	3.64
$\langle S^2 \rangle$ ^[c]	2.89	6.02

[a] The experimental values are given in parentheses. [b] The total spin density at the iron ion including s and p orbitals. [c] The expectation value of the total spin squared operator S^2 .

The results of the geometry optimization of the dianion in **2** are shown in Table 2. The calculated bond lengths within the pda ligands and the C–N bonds are in very good agreement with the experimental values, while the Fe–N distances are underestimated in the calculations by an average of 0.007 Å. This unusual behavior for the B3LYP functional, which typically overestimates metal–ligand bond lengths,^[27] may result from the 9° increased planarity of the optimized structure. A population analysis yields a total spin density of 3.64 located at the iron atom, and of 0.36 located at the ligands, predominately at the N-donor atoms (Figure 15). This is representative of a high-spin configuration for the Fe^{II} ion (Figure 16). Although the isomer shift is satisfactorily reproduced by our calculations ($\delta_{\text{calcd}} = 0.63$, $\delta_{\text{exptl}} =$

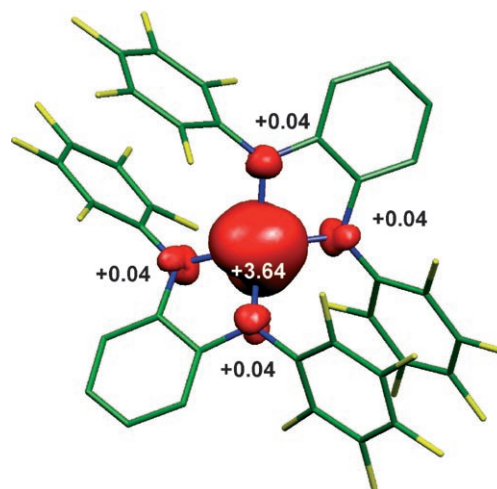


Figure 15. Spin density map for $[\text{Fe}^{\text{II}}(\text{pda}^{2-})_2]^{2-}$ in **2** and **3^{LT}**.

Table 3. Reduced orbital charges and orbital spin densities calculated for **1–3**.

	1		2		Dication in 3^{LT}		Monocation in 3^{HT}		Dianion in 3^{LT}		Monoanion in 3^{HT}	
	Electron	Spin	Electron	Spin	Electron	Spin	Electron	Spin	Electron	Spin	Electron	Spin
d_{z^2}	1.10	0.89	1.06	0.93	0.64	0	1.26	0.85	1.06	0.93	1.11	0.88
d_{xz}	1.27	0.68	1.17	0.87	1.87	0	1.44	0.53	1.17	0.87	1.35	0.70
d_{yz}	1.11	0.90	1.07	0.94	1.83	0	1.28	0.70	1.07	0.94	1.13	0.88
$d_{x^2-y^2}$	1.97	0.01	1.94	0.03	0.63	0	1.26	0.84	1.94	0.03	1.97	0.01
d_{xy}	1.02	0.33	1.24	0.79	1.89	0	1.24	0.74	1.24	0.79	0.92	0.18
Σd_i	6.46	2.82	6.48	3.55	6.86	0	6.49	3.67	6.48	3.55	6.47	2.65
Fe_{total} ^[a]		2.92		3.64		0		3.68		3.64		2.72
L_{total} ^[b]		-0.92 ^[c]		0.36		0		-0.68 ^[c]		0.36		0.28

[a] The total spin density at the iron ion including s and p orbitals. [b] The total spin density at the ligands. [c] A broken symmetry solution.

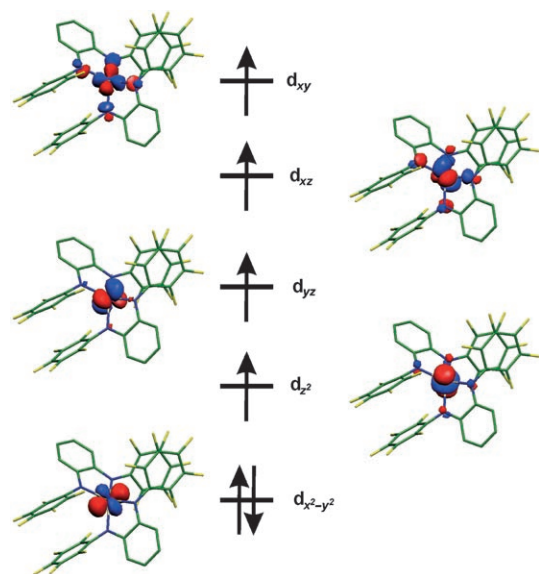


Figure 16. Qualitative MO scheme for the dianion in **2** and **3^{LT}**.

0.72 mms^{-1}), the calculated quadrupole splitting is significantly larger than experimentally observed ($\Delta E_{\text{Qcalcd}} = 5.35$, $\Delta E_{\text{Qexptl}} = 3.07 \text{ mms}^{-1}$). As we have pointed out above, the quadrupole splitting in the dianion is very sensitive to the twist angle. Consequently, the observed deviation may arise from the imperfectly reproduced dihedral angle. When the twist angle was artificially decreased from 45° to 40° , the quadrupole splitting constant decreased by 20%.

It is worthwhile to compare the charge and spin density at the iron centers in **1** and **2**. As commonly observed for population analysis, irrespective of the oxidation state of the iron center, the Löwdin orbital charges in **1** and **2** are very similar and correspond to ≈ 6.5 d electrons (Table 3). The overestimation by ≈ 1.5 electrons for the ferric complex **1** and by ≈ 0.5 electrons for the ferrous complex **2** results from the varying degrees of covalency. However, the Löwdin orbital spin densities are significantly different for **1** and **2**; the spin density of 2.82 located at the iron d orbitals confirms the intermediate-spin Fe^{III} center in **1**, while the d-orbital spin density of 3.55 corresponds to the high-spin Fe^{II} ion in **2**. The difference in the total spin density is reflected by the d_{xy} orbital spin density changing from 0.33 in **1** to 0.79 in **2**. Thus, the formally empty d_{xy} iron orbital in **1** ac-

quires considerable spin density (+0.33) by spin-polarized σ donation from the filled ligand orbitals; however, the formally singly occupied d_{xy} orbital in **2** loses inherent spin density (-0.21) by σ donation from the filled ligand orbitals. In both cases covalent bonding is the origin of the variation in orbital spin density. Since all metal d orbitals experience some deviation from the ideal spin densities of 0 or 1, the value of the spin density summed over all metal d-orbitals may produce much higher deviations than seen for one single orbital. Thus, care should be taken when defining electronic configurations based on the total metal spin density.

Density functional theory (DFT) calculations of **3^{LT}** and **3^{HT}**:

The geometry optimization of the cations and the anions in **3^{LT}** and **3^{HT}** were performed separately, with the B3LYP functional used for the cations, and the B3LYP with empirical Van der Waals corrections implemented for the anions. The following ground states were imposed: $S=0$ for the dication and $S=2$ for the dianion in **3^{LT}**, and $S=3/2$ for both the monocation and the monoanion in **3^{HT}**. All significant geometrical features were closely reproduced in the calculations (Table 5). The intramolecular π - π interactions in the anions are nicely reproduced resulting in dihedral angles close to the experiment. The optimized dication, $[\text{Fe}^{\text{II}}(\text{dad}^0)_3]^{2+}$ in **3^{LT}**, displays short C=N and long C-C bonds within the three dad ligands in agreement with the fully oxidized level of the ligands, and relatively short Fe-N distances resulting from the low-spin configuration of the iron center. The Fe-N distances in the monocation $[\text{Fe}^{\text{II}}(\text{dad}^-)_2(\text{dad}^-)]^+$ are significantly longer as the iron ion possesses a high-spin configuration in **3^{HT}**, while the elongation of the C=N and the shortening of the C-C bonds within one dad ligand indicates the acquired π -radical character of the latter. No significant changes in the calculated bond lengths within the pda ligands are observed on conversion of the dianion $[\text{Fe}^{\text{II}}(\text{pda}^{2-})_2]^{2-}$ to the monoanion $[\text{Fe}^{\text{III}}(\text{pda}^{2-})_2]^-$. However, following the experimental observations,^[9] the Fe-N bonds are significantly shorter in the monoanion than in the dianion. Geometry optimizations of the dianion $[\text{Fe}^{\text{II}}(\text{pda}^{2-})_2]^{2-}$ started from the two different crystal structures **2** and **3^{LT}** converged to a single solution.

According to the population analysis the electronic configuration of the iron in the dianion in **3^{LT}** is $(d_{x^2-y^2})^2(d_{z^2})^1(d_{yz})^1(d_{xz})^1(d_{xy})^1$, that is, a high-spin Fe^{II} ion (Table 3). Upon

Table 5. Geometry optimization of **3^{LT}** and **3^{HT}** performed with the B3LYP functional for the cations and the B3LYP+vdw for the anions.

	Dication in 3^{LT}		Monocation in 3^{HT}			Dianion in 3^{LT}		Monoanion in 3^{HT}	
	calcd	exptl ^[a]	calcd	exptl ^[a]		calcd	exptl ^[a]	calcd	exptl ^[a]
Fe2-N21	2.046	1.983(2)	2.202	2.127(5)	Fe1-N1	2.027	1.996(2)	1.914	1.890(5)
Fe2-N24	2.043	1.973(2)	2.216	2.143(6)	C2-N1	1.391	1.399(4)	1.399	1.403(7)
Fe2-N41	2.046	1.976(2)	2.163	2.092(5)	C2-C3	1.404	1.391(4)	1.400	1.378(8)
C22=N21	1.294	1.307(3)	1.301	1.318(8)	C3-C4	1.404	1.394(4)	1.403	1.394(8)
C23=N24	1.294	1.301(3)	1.299	1.297(7)	C4-C5	1.398	1.364(4)	1.398	1.386(10)
C42=N41	1.294	1.296(4)	1.318	1.350(7)	C2-C7	1.444	1.428(4)	1.427	1.387(8)
C22-C23	1.493	1.473(4)	1.484	1.463(8)	α , ^[b] °	54.7	57.1	44.9	52.7
C42-C42'	1.493	1.472(5)	1.458	1.412(11)					

[a] The averaged values are given. [b] The dihedral angle between the two $\text{C}_6\text{H}_4\text{N}_2\text{Fe}$ planes.

oxidation, the d_{xy} orbital, which is σ antibonding with respect to the ligands, becomes unoccupied, which corresponds to a change to an intermediate-spin Fe^{III} ion in $\mathbf{3}^{\text{HT}}$. The total spin densities of 3.64 and 2.72 located at the iron centers in $\mathbf{3}^{\text{LT}}$ and $\mathbf{3}^{\text{HT}}$, respectively, confirm the presence of the high-spin Fe^{II} and the intermediate-spin Fe^{III} ions in the corresponding anions (Figures 15 and 17). The electronic

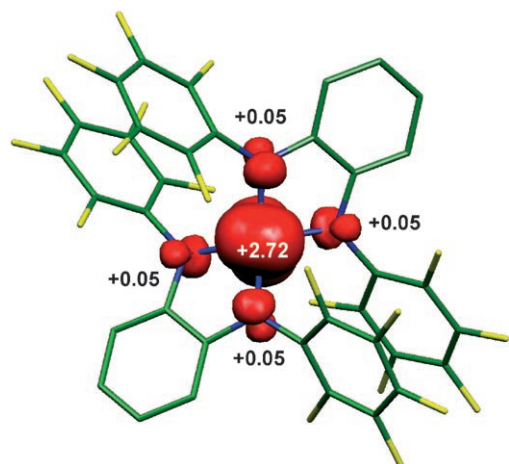


Figure 17. Spin density map for $[\text{Fe}^{\text{III}}(\text{pda}^{2-})_2]^-$ in $\mathbf{3}^{\text{HT}}$.

configuration of the iron ion in the near-octahedral dication in $\mathbf{3}^{\text{LT}}$ is $(t_{2g})^6(e_g)^0$, that is, a diamagnetic low-spin Fe^{II} ion. One electron reduction of a dad ligand in the monocation in $\mathbf{3}^{\text{HT}}$ transformed the spin state of the iron to the high-spin ferrous configuration $(t_{2g})^4(e_g)^2$, affording a spin density of 3.68.

The lowest energy solution for the monocation in $\mathbf{3}^{\text{HT}}$ is the BS(4,1), which corresponds to an electronic structure of a high-spin Fe^{II} ion coupled antiferromagnetically to one ligand radical dad^- (Figure 18). The high-spin state $M_S = 5/2$ is destabilized relative to the BS solution by 11 kcal mol $^{-1}$. The overlap integral $S_{\text{AB}} = 0.67$ shows slightly decreased diradical character of the coupled magnetic pair when compared to $\mathbf{1}$ (vide supra), while the AF coupling given by $J = -922 \text{ cm}^{-1}$ is stronger. The AF coupling can be nicely visualized by the BS spin density map shown in Figure 19. Positive spin density is mainly centered at the metal ($\rho_{\text{Fe}} = +3.68$) and negative spin density is essentially localized on one dad ligand ($\rho_{\text{L}} = -0.68$). Slight delocalization of the π radical ligand results from the non-ideal octahedral geometry, as shown by the dihedral angles of 77.9, 90.0, and 81.5° between the ligand planes.

The Mössbauer parameters calculated for all four ions in $\mathbf{3}^{\text{LT}} \rightleftharpoons \mathbf{3}^{\text{HT}}$ are summarized in Table 6. Very good agreement between the calculated and the experimental values is achieved for the isomer shift and quadrupole splitting, but less so for the asymmetry parameter. The absolute value of the quadrupole splitting for the dianion in $\mathbf{3}^{\text{LT}}$ is very well predicted by our calculations (deviation of 3%); however, the sign of the quadrupole splitting is not reproduced. It is positive in the calculations, but negative in the experiment, and

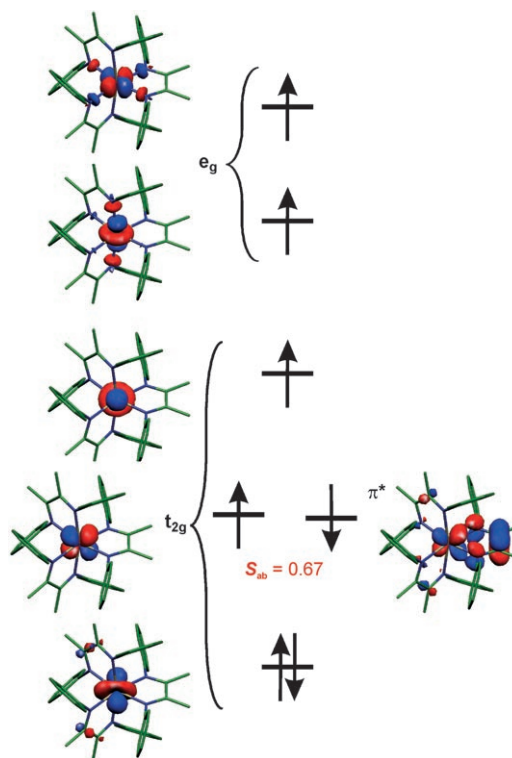


Figure 18. Qualitative MO scheme for $[\text{Fe}^{\text{II}}(\text{dad}^0)_2(\text{dad}^-)]^+$ in $\mathbf{3}^{\text{HT}}$; S_{ab} is an overlap integral for the pair of magnetic orbitals.

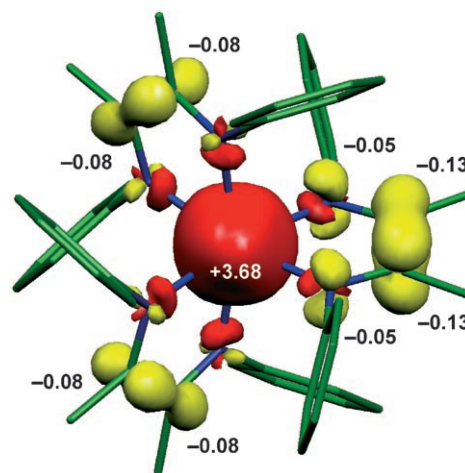


Figure 19. Broken symmetry spin density map for $[\text{Fe}^{\text{II}}(\text{dad}^0)_2(\text{dad}^-)]^+$ in $\mathbf{3}^{\text{HT}}$.

neither the calculated, nor the experimental asymmetry parameter approaches unity. Assuming that the quadrupole splitting in the twisted dianion is highly sensitive to the complex geometry, we calculated the Mössbauer spectrum of the non-optimized structure of $\mathbf{3}^{\text{LT}}$. The isomer shift and the quadrupole splitting ($\delta = 0.57$, $\Delta E_Q = +5.25 \text{ mm s}^{-1}$) closely matched the experimental values, though the sign of the quadrupole splitting remained positive, the asymmetry parameter $\eta = 0.9$, approaches unity, thus making the sign of the calculated quadrupole splitting ambiguous. We believe

Table 6. Calculation of properties for 3^{LT} and 3^{HT} .

	Dication in 3^{LT}	Monocation in 3^{HT}	Dianion in 3^{LT}	Monoanion in 3^{HT}
δ [mm s ⁻¹]	0.51 (0.38) ^[a]	0.86 (0.76)	0.63 (0.68)	0.19 (0.16)
ΔE_O [mm s ⁻¹]	-0.49 (-0.53)	1.98 (1.80) ^[b]	5.36 (-5.20)	3.84 (4.19) ^[b]
η	0.02 (0.0)	0.35	0.46 (0.30)	0.37
$\rho_{Fe}^{[c]}$	0	3.68	3.64	2.72
$\langle S^2 \rangle^{[d]}$	0	4.61	6.02	3.82

[a] The experimental values are given in parentheses. [b] The sign of ΔE_O was not determined experimentally. [c] The total spin density at the iron ion including *s* and *p* orbitals. [d] The expectation value of the total spin-squared operator S^2 .

that the high-spin Fe^{II} ion in the dianion in 3^{LT} possesses a negative quadrupole splitting as derived from the experiment.

Calculation of the electric-field gradient (EFG) tensors: The neutral complex **1** and the monoanion in 3^{HT} are rare examples^[7] of four-coordinate intermediate-spin Fe^{III} complexes. Ferric species of intermediate-spin are more common for five-coordinate square-pyramidal^[6,14] and six-coordinate distorted octahedral species of C_{4v} symmetry.^[30] According to simple considerations from crystal field (CF) theory, the valence contribution to the EFG at an intermediate-spin Fe^{III} center should vanish with a resulting quadrupole splitting close to zero.^[31] In contrast, we observe $\Delta E_O = 4.45$ mm s⁻¹ for **1** and $|\Delta E_O| = 4.19$ mm s⁻¹ for the anion in 3^{HT} . Although a large quadrupole splitting is not unexpected for the high-spin Fe^{II} ion, the large $\Delta E_O = -5.20$ mm s⁻¹ observed for the dianion in 3^{LT} is surpassed in the ⁵⁷Fe Mössbauer spectroscopy by only two complexes, namely [(PhB{CH₂P(*i*Pr)₂})₃Fe^{IV}≡N] and [(PhB{CH₂P(CH₂Cy)₂})₃Fe^{IV}≡N].^[32] However, no explanation has been given for the origin of the observed $\Delta E_O = 6.01$ mm s⁻¹.^[32] Very recently Meyer et al. reported on an Fe^{IV}-nitrido complex that shows even larger quadrupole splitting ΔE_O of 6.04(1) mm s⁻¹.^[33]

In this work the largest component of the total principle EFG tensor, by definition V_{zz} , is designated as q . The total EFG tensor may be decomposed into the partial EFG tensors, which are projected into the coordinate system of the total EFG tensor. The v_{zz} , a projection of the partial EFG tensor into the principle *z* axis of the total EFG tensor, is labeled as q_i . Generally, q may be decomposed according to Equation (2),^[34] in which q_{loc} is a local contribution of the orbitals with non-zero iron character, q_{lat} is a lattice (ligand) contribution arising from the net charges on the distant atoms around an iron center, q_{bond} originates from the electron density in the bonds between the iron ion and ligand atoms, and $q_{3center}$ arises from the electron density in the bonds which do not include the iron ion.

$$q = q_{loc} + q_{lat} + q_{bond} + q_{3center} \quad (2)$$

The results of the decomposition of the EFG tensors for **1** and the anions in **3** are shown in Table 7. In all cases the local contribution is the largest component and comprises

Table 7. Decomposition of $q = V_{zz}$ component of the total EFG tensor at iron centers [in au⁻³].^[a]

	1	Monoanion in 3^{HT}	Dianion in 3^{LT}
q_{loc}	2.483	2.103	3.084
q_{lat}	0.005	0.005	0.012
q_{bond}	0.148	0.207	0.096
$q_{3center}$	-0.007	-0.004	-0.001
q	2.629	2.311	3.191

[a] To convert q into quadrupole splitting constant: ΔE_O [mm s⁻¹] = $1.6195q(1+1/3\eta^2)^{1/2}$.

91–97% of q . The lattice and the three-center components are small and of opposite sign; they virtually cancel each other in **1** and in the monoanion in 3^{HT} . The bond contribution is the second largest component of the EFG and has the same sign as q_{loc} , which amplifies the already large EFG produced by the local component.

The local component q_{loc} can be analyzed further by consideration of the contribution of Pipek–Mezey localized orbitals (LOs) to the EFG. The LOs with predominant iron or nitrogen character were found to account for 92–97% of the total q_{loc} ; this main contribution is labeled as q'_{loc} . After the orbital composition of the LO's were analyzed we could decompose q'_{loc} further according to Equation (3), in which q_{core} is a contribution from the deformed iron core orbitals (1s, 2s, and 2p), q_{val} arises from the valence shell of the iron (3s, 3p, and 3d), q_{cov} is a contribution from predominantly ligand based LOs with some metal character, and q_{lig} arises from the highly covalent LOs of N–C bonds.

$$q'_{loc} = q_{core} + q_{val} + q_{cov} + q_{lig} \quad (3)$$

Both intermediate-spin ferric species, **1** and the monoanion in 3^{HT} , show very similar components in the decomposition, unlike the high-spin ferrous dianion in 3^{LT} (Table 8).

Table 8. Decomposition of the truncated^[a] local component q'_{loc} of the total EFG tensor at iron centers [in au⁻³].^[b]

	1	Monoanion in 3^{HT}	Dianion in 3^{LT}
q_{core}	0.20	0.14	0.31
q_{val}	0.61	0.71	2.62
q_{cov}	1.36	0.82	0.23
q_{lig}	0.24	0.26	-0.10
q'_{loc}	2.41	1.93	3.06

[a] Restricted to the iron and nitrogen orbitals. [b] To convert q into quadrupole splitting constant: ΔE_O [mm s⁻¹] = $1.6195q(1+1/3\eta^2)^{1/2}$.

The core (q_{core}) and the ligand (q_{lig}) components are the smallest components, each generally contributing less than 10% to q'_{loc} . The valence iron contribution q_{val} is very large for the high-spin ferrous dianion in 3^{LT} in line with CF theory: an aspherical population of d orbitals in a high-spin d⁶ configuration leads to a large EFG. In contrast, q_{val} for **1** and for the monoanion in 3^{HT} are considerably smaller, but do not vanish, mainly because of the anisotropic population of the valence d and p orbitals of the iron ion. Surprisingly, in **1** and in the monoanion in 3^{HT} , the covalent contribution

q_{cov} is very large; it is of nearly the same value as q_{val} in the monoanion in **3^{HT}** and more than twice as large as q_{val} in **1**. It is most remarkable that for all three species the valence and the covalence components of the EFG have the same sign. Thus, the covalent bonding between the iron and the ligand donors does not reduce the EFG as anticipated,^[35] but in fact significantly increases the EFG. This increase results in the large quadrupole splitting observed for the intermediate-spin Fe^{III} ions in **1** and in the monoanion of **3^{HT}**, and the huge quadrupole splitting for the high-spin Fe^{II} ion in the dianion in **3^{LT}**. The origin of the very large $q_{\text{cov}}=1.36 \text{ au}^{-3}$ in **1** relative to the smaller $q_{\text{cov}}=0.82 \text{ au}^{-3}$ in the monoanion in **3^{HT}** derives from the significant iron d_{xy} character of one ligand orbital in **1**. (Table 3).

The orientation of the principle EFG tensors in the molecular structures of **1** and the monoanion in **3^{HT}** are shown in Figure 20. In both cases the coordinate system of the prin-

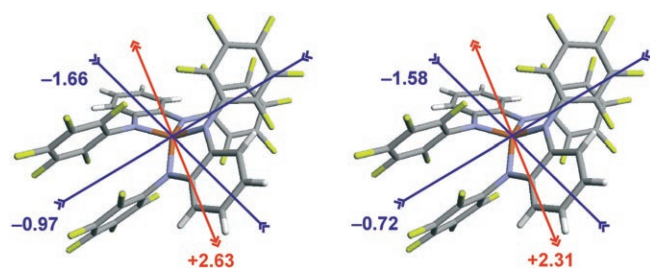


Figure 20. Calculated orientation of the EFG tensor in the molecular structure of **1** (left) and the monoanion in **3^{HT}** (right).

ciple EFG tensor is collinear with the three mutually perpendicular C_2 axes of the nearly D_2 symmetrical $[\text{Fe}(\text{pda})_2]^n$ unit. The principal z axis is perpendicular to the four-nitrogen-atom plane, and the principle y axis is coincident with the local C_2 axes of each ligand. Due to the uncertainty in the sign of the quadrupole splitting and the value of the asymmetry parameter for the dianion in **3^{LT}**, the orientation of its principle EFG tensor is not shown, but we expect it to have the principle z axis perpendicular to the N_4 -plane similar to **1** and **3^{HT}**.

Conclusion

The neutral complex $[\text{Fe}^{\text{III}}(\text{pda}^{2-})(\text{pda}^{\cdot-})]^0$ (**1**) is composed of a four-coordinate intermediate-spin Fe^{III} ion ($S_{\text{Fe}}=3/2$) antiferromagnetically coupled to one π -radical ligand ($S_{\text{R}}=1/2$) as shown by the experimental and theoretical studies. It can reversibly be oxidized twice or reduced twice, that is, **1** is the central member of the $[\text{Fe}(\text{pda})_2]^{2+/1+0/1-2-}$ redox series. The doubly reduced species has been isolated as $[\text{AsPh}_4]_2[\text{Fe}^{\text{II}}(\text{pda}^{2-})_2]$ (**2**) and crystallographically characterized. The dianion in **2** consists of a high-spin ferrous ion ($S_{\text{Fe}}=2$) and two closed-shell dianionic pda^{2-} ligands. The third member of the redox series, the singly reduced $[\text{Fe}^{\text{III}}(\text{pda}^{2-})_2]^-$, which has been reported previously in the coor-

dination salt $[\text{Fe}(\text{dad})_3][\text{Fe}(\text{pda})_2]$ (**3**; **3^{LT}** is a low-temperature form and **3^{HT}** is a high-temperature form), contains an intermediate-spin ferric ion ($S_{\text{Fe}}=3/2$) and two closed-shell dianionic ligands. Due to four strongly electron-withdrawing $N\text{-C}_6\text{F}_5$ substituents, the redox potentials for $[\text{Fe}(\text{pda})_2]^{2+/1+0/1-2-}$ are all shifted towards positive voltages, which stabilizes reduced and destabilizes oxidized species. The large quadrupole splitting in ⁵⁷Fe Mössbauer spectra observed for the intermediate-spin Fe^{III} ions in **1** and **3^{HT}**, and the extraordinarily large quadrupole splitting observed for the high-spin Fe^{II} ion in **3^{LT}** results from covalent bonding between the iron and the ligand donors, in which the valence contribution to the electric field gradient is not reduced, but significantly increased by the covalence contribution.

Experimental Section

N,N'-Bis(pentafluorophenyl)-*o*-phenylenediamine (H_2pda) was prepared according to a reported procedure.^[10] *n*-Butyllithium (1.6 M solution in *n*-hexane) and $[\text{AsPh}_4]\text{Cl}$ were purchased from Aldrich. All syntheses were performed under a dry, oxygen-free argon atmosphere by using standard Schlenk techniques and dried solvents.

$[\text{Fe}^{\text{III}}(\text{pda}^{2-})(\text{pda}^{\cdot-})]$ (1**):** *n*BuLi (3.9 mL, 6.24 mmol) was slowly added at -50°C to a solution of H_2pda (1.38 g, 3.13 mmol) in diethyl ether (30 mL). After stirring for 15 min, a suspension of FeCl_2 (0.20 g, 1.58 mmol) in THF (15 mL) was added through a cannula and the reaction mixture was allowed to warm to RT. The reaction mixture was stirred overnight, during which time the color changed from yellow to orange. A solution of FeCl_3 (0.51 g, 3.14 mmol) in THF (5 mL) was then added to the reaction mixture, cooled to 0°C . The reaction mixture was then stirred for 1 h at RT, all volatiles were removed in vacuo, and the residue was extracted with toluene (120 mL) and recrystallized from a Et_2O /toluene mixture (2:1). The air- and moisture-sensitive dark blue-green crystals, which were suitable for X-ray crystallography, were washed with cold *n*-pentane and dried in vacuo. Yield: 1.02 g (70%); HR EI-MS: m/z calcd: 931.9779; found: 931.9816 $[M]^+$; elemental analysis calcd (%) for $\text{C}_{36}\text{H}_8\text{F}_{20}\text{N}_4\text{Fe}$: C 46.38, H 0.86, N 6.01; found: C 46.00, H 0.79, N 6.16.

$[\text{AsPh}_4]_2[\text{Fe}^{\text{II}}(\text{pda}^{2-})_2]$ (2**):** *n*BuLi (0.56 mL, 0.896 mmol) was slowly added to a solution of H_2pda (200 mg, 0.454 mmol) in THF (2.5 mL) maintained at -50°C . After the yellow solution was stirred for 10 min anhydrous FeCl_2 (28.8 mg, 0.227 mmol) suspended in THF (2.5 mL) was added. The reaction mixture was stirred for 1 h at RT, afterwards well-dried $[\text{AsPh}_4]\text{Cl}$ (190 mg, 0.454 mmol) suspended in THF (2.5 mL) was added with vigorous stirring. The bright-orange crystals appeared during the first 10 min of stirring. After the reaction mixture was kept at $+4^\circ\text{C}$ for several hours, a red solution was decanted, and an orange crystalline product was dried in vacuo. The yield of the raw product was 293 mg. The solid was then recrystallized from a toluene/acetonitrile mixture (16:5.5 mL) to get bright-orange extremely sensitive crystals suitable for X-ray crystallography. Yield: 221 mg (57%). ESI-MS (MeCN): m/z : 932 $[\text{Fe}(\text{pda})_2]^-$, 383 $[\text{AsPh}_4]^+$; elemental analysis calcd (%) for $\text{C}_{112}\text{H}_{80}\text{As}_2\text{F}_{20}\text{FeN}_4$: C 65.06, H 3.90, N 2.71, Fe 2.70; found: C 64.82, H 4.11, N 2.68, Fe 2.63.

Physical measurements: ESI-MS spectra were obtained on a Finnigan MAT 95 spectrometer. High-resolution mass spectra were obtained on a Finnigan MAT 95S mass spectrometer (70 eV, EI). Cyclic voltammograms were recorded with an EG&G potentiostat/galvanostat. Electronic spectra were recorded with a Perkin-Elmer double-beam UV/VIS/NIR spectrometer Lambda 19 (300–2000 nm). Temperature-dependent magnetic susceptibility data were recorded on an MPMS Quantum Design SQUID magnetometer in the temperature range 2–300 K. The experi-

mental magnetic susceptibility data were corrected for underlying diamagnetism and temperature-independent paramagnetism. Mössbauer data were recorded on alternating constant-acceleration spectrometers. The sample temperature was maintained constant in an Oxford Instruments Variox cryostat or an Oxford Instruments Mössbauer-Spectromag cryostat. The latter was used for measurement in applied magnetic fields with the field oriented perpendicular to the γ -beam. Isomer shifts are given relative to α -Fe at room temperature. Elemental analyses were performed by the Microanalytical Laboratory, Mülheim an der Ruhr (Germany).

X-ray crystallographic data collection and refinement of the structures:

A dark green single crystal of **1** and an orange crystal of **2** were coated with perfluoropolyether, picked up with nylon loops and were immediately mounted in the nitrogen cold stream of a Bruker-Nonius KappaCCD diffractometer equipped with a Mo-target rotating-anode X-ray source and a graphite monochromator ($\lambda = 0.71073 \text{ \AA}$). Final cell constants were obtained from least-squares fits of all measured reflections. Intensity data were corrected for absorption using intensities of redundant reflections. The structures were readily solved by Patterson methods and subsequent difference Fourier techniques. The Siemens SHELXTL^[36] software package was used for solution and refinement of the structures. All non-hydrogen atoms were anisotropically refined and hydrogen atoms were placed at calculated positions and refined as riding atoms with isotropic displacement parameters. Crystallographic data of the compounds are listed in Table 9.

Table 9. Crystallographic data for **1** and **2**.

	1·Et ₂ O	2·4 C ₇ H ₈
formula	C ₄₀ H ₁₈ F ₂₀ FeN ₄ O	C ₁₁₂ H ₈₀ As ₂ F ₂₀ FeN ₄
crystal size [mm]	0.10 × 0.08 × 0.02	0.32 × 0.07 × 0.05
M_r	1006.43	2067.49
crystal system	monoclinic	orthorhombic
space group	$P2_1/n$ (No. 14)	$Fdd2$ (No. 43)
a [Å]	8.5878(5)	29.301(2)
b [Å]	28.060(2)	64.319(5)
c [Å]	15.3071(9)	9.7682(7)
β [°]	92.950(5)	
V [Å ³]	3683.7(4)	18409(2)
Z	4	8
T [K]	100(2)	100(2)
ρ_{calc} [g cm ⁻³]	1.815	1.492
μ (MoK α) [mm ⁻¹]	0.554	0.972
reflns collected/ θ_{max}	51008/27.50	22542/24.71
unique reflns/ $I > 2\sigma(I)$	8434/6084	7600/5658
no. params/restraints	597/0	629/1
goodness of fit	1.126	1.043
$R1$ [$I > 2\sigma(I)$]	0.0541	0.0553
$wR2$ [$I > 2\sigma(I)$]	0.1027	0.1030

Calculations: The program package ORCA 2.6 revision 04 was used for all calculations.^[37] Geometry optimization for all complexes were performed with the B3LYP functional,^[21] and additionally with PW91,^[20] BP86,^[18,19] and B3P86^[18] functionals for **1**. Empirical Van der Waals (VDW) corrections^[38] were used for geometry optimization of **1** and anions in **2** and **3**. The triple- ζ basis sets with one-set of polarization functions^[39] (TZVP) were used for the iron and nitrogen atoms, and the double- ζ basis sets with one-set of polarization functions^[40] (SVP) were used for all other atoms. The resolution of the identity approximation (RI/RIJONX) was employed^[41,42] with matching auxiliary basis sets.^[42] Convergence criteria for geometry optimization were set to default values (OPT), and “tight” convergence criteria were used for SCF calculations (TIGHTSCF). Electronic energies and properties were calculated with the B3LYP functional with the same basis sets and SCF convergence criteria as for geometry optimization. Broken symmetry solutions were analyzed with the corresponding orbital transformation.^[28,43] For calculation of Mössbauer parameters, the “core” CP(PPP) basis set for iron^[29,44]

with enhanced integration accuracy on the iron (SpecialGridIntAcc 7) were used. High-spin states were calculated on the high-spin geometries, when the exchange coupling constants were estimated.^[26] All reduced orbital charges and spin densities were calculated according to Löwdin population analysis.^[45] Orbitals and spin densities were visualized with the program Molekel.^[46]

Acknowledgements

Prof. Dr. F. Neese, Dr. S. Ye, and Dr. T. Petrenko (Universität Bonn, Germany) are acknowledged for their helpful suggestions and comments concerning DFT calculations. A. Göbels, H. Schucht, and B. Mienert are acknowledged for measurements. M.M.K. is grateful to the Max Planck Society for a postdoctoral fellowship.

- [1] a) J. Bollinger, J. Martin, C. Krebs, *J. Inorg. Biochem.* **2006**, *100*, 586; b) H.-P. Hersleth, U. Ryde, P. Rydberg, C. H. Gorbitz, K. K. Andersson, *J. Inorg. Biochem.* **2006**, *100*, 460; c) B. A. Jazdzewski, W. B. Tolman, *Coord. Chem. Rev.* **2000**, *200–202*, 633; d) W. Kaim, *Dalton Trans.* **2003**, 761; e) G. H. Loew, D. L. Harris, *Chem. Rev.* **2000**, *100*, 407; f) W. Nam, *Acc. Chem. Res.* **2007**, *40*, 522; g) M. S. Rogers, D. M. Dooley, *Curr. Opin. Chem. Biol.* **2003**, *7*, 189; h) J. Stubbe, W. A. van der Donk, *Chem. Rev.* **1998**, *98*, 705; i) F. Thomas, *Eur. J. Inorg. Chem.* **2007**, 2379; j) J. W. Whittaker, *Chem. Rev.* **2003**, *103*, 2347; k) P. Chaudhuri, K. Wieghardt, *Prog. Inorg. Chem.* **2001**, *50*, 151; l) W. Kaim, B. Schwederski, *Pure Appl. Chem.* **2004**, *76*, 351.
- [2] a) K. J. Blackmore, J. W. Ziller, A. F. Heyduk, *Inorg. Chem.* **2005**, *44*, 5559; b) S. C. Bart, E. Lobkovsky, E. Bill, P. J. Chirik, *J. Am. Chem. Soc.* **2006**, *128*, 5302; c) S. C. Bart, A. C. Bowman, E. Lobkovsky, P. J. Chirik, *J. Am. Chem. Soc.* **2007**, *129*, 7212; d) P. Chaudhuri, K. Wieghardt, T. Weyhermüller, T. K. Paine, S. Mukherjee, C. Mukherjee, *Biol. Chem.* **2005**, *386*, 1023; e) M. R. Haneline, A. F. Heyduk, *J. Am. Chem. Soc.* **2006**, *128*, 8410; f) G. D. Jones, J. L. Martin, C. McFarland, O. R. Allen, R. E. Hall, A. D. Haley, R. J. Brandon, T. Konovalova, P. J. Desrochers, P. Pulay, D. A. Vicio, *J. Am. Chem. Soc.* **2006**, *128*, 13175; g) Q. Knijnenburg, S. Gambarotta, P. H. M. Budzelaar, *Dalton Trans.* **2006**, 5442; h) C. Mukherjee, T. Weyhermüller, E. Bothe, P. Chaudhuri, *C. R. Chim.* **2007**, *10*, 313; i) C. Stanciu, M. E. Jones, P. E. Fanwick, M. M. Abu-Omar, *J. Am. Chem. Soc.* **2007**, *129*, 12400; j) K. J. Blackmore, N. Lal, J. W. Ziller, A. F. Heyduk, *J. Am. Chem. Soc.* **2008**, *130*, 2728; k) H. Grützmacher, *Angew. Chem.* **2008**, *120*, 1838; *Angew. Chem. Int. Ed.* **2008**, *47*, 1814; l) M. R. Ringenberg, S. L. Kokatam, Z. M. Heiden, T. B. Rauchfuss, *J. Am. Chem. Soc.* **2008**, *130*, 788; m) C. J. Rolle, K. I. Hardcastle, J. D. Soper, *Inorg. Chem.* **2008**, *47*, 1892; n) M. W. Bouwkamp, A. C. Bowman, E. Lobkovsky, P. J. Chirik, *J. Am. Chem. Soc.* **2006**, *128*, 13340.
- [3] a) A. Bencini, A. Caneschi, A. Dei, D. Gatteschi, C. Sangregorio, D. Shultz, L. Sorace, M. G. F. Vaz, *C. R. Chim.* **2003**, *6*, 663; b) A. Dei, D. Gatteschi, C. Sangregorio, L. Sorace, *Acc. Chem. Res.* **2004**, *37*, 827; c) E. Evangelio, D. Ruiz-Molina, *Eur. J. Inorg. Chem.* **2005**, *2005*, 2957; d) D. Gatteschi, *Adv. Mater.* **1994**, *6*, 635; e) D. N. Hendrickson, C. G. Pierpont, *Top. Curr. Chem.* **2004**, *234*, 63; f) T. Hirao, *Coord. Chem. Rev.* **2002**, *226*, 81; g) J. S. Miller, A. J. Epstein, *Coord. Chem. Rev.* **2000**, *206–207*, 651; h) O. Sato, A. Cui, R. Matsuda, J. Tao, S. Hayami, *Acc. Chem. Res.* **2007**, *40*, 361; i) M. D. Ward, J. A. McCleverty, *J. Chem. Soc. Dalton Trans.* **2002**, 275.
- [4] K. Ray, T. Petrenko, K. Wieghardt, F. Neese, *Dalton Trans.* **2007**, 1552.
- [5] N. Muresan, C. C. Lu, M. Ghosh, J. C. Peters, M. Abe, L. M. Henling, T. Weyhermüller, E. Bill, K. Wieghardt, *Inorg. Chem.* **2008**, *47*, 4579.
- [6] K. Chlopek, E. Bill, T. Weyhermüller, K. Wieghardt, *Inorg. Chem.* **2005**, *44*, 7087.

- [7] a) J. Bachmann, D. G. Nocera, *J. Am. Chem. Soc.* **2005**, *127*, 4730; b) D. Bhattacharya, S. Dey, S. Maji, K. Pal, S. Sarkar, *Inorg. Chem.* **2005**, *44*, 7699.
- [8] A. L. Balch, R. H. Holm, *J. Am. Chem. Soc.* **1966**, *88*, 5201.
- [9] M. M. Khusniyarov, T. Weyhermüller, E. Bill, K. Wieghardt, *Angew. Chem.* **2008**, *120*, 1248; *Angew. Chem. Int. Ed.* **2008**, *47*, 1228.
- [10] M. M. Khusniyarov, K. Harms, O. Burghaus, J. Sundermeyer, B. Sarkar, W. Kaim, J. van Slageren, C. Duboc, J. Fiedler, *Dalton Trans.* **2008**, 1355.
- [11] M. M. Khusniyarov, K. Harms, O. Burghaus, J. Sundermeyer, *Eur. J. Inorg. Chem.* **2006**, 2985.
- [12] D. Herebian, E. Bothe, F. Neese, T. Weyhermüller, K. Wieghardt, *J. Am. Chem. Soc.* **2003**, *125*, 9116.
- [13] a) V. Taberner, M. C. Maestre, G. Jimenez, T. Cuenca, C. Ramirez de Arellano, *Organometallics* **2006**, *25*, 1723; b) V. Taberner, T. Cuenca, E. Herdtweck, *Eur. J. Inorg. Chem.* **2004**, 3154; c) D. J. Darensbourg, K. K. Klausmeyer, J. H. Reibenspies, *Inorg. Chem.* **1996**, *35*, 1535.
- [14] a) A. K. Patra, E. Bill, T. Weyhermüller, K. Stobie, Z. Bell, M. D. Ward, J. A. McCleverty, K. Wieghardt, *Inorg. Chem.* **2006**, *45*, 6541; b) K. Ray, E. Bill, T. Weyhermüller, K. Wieghardt, *J. Am. Chem. Soc.* **2005**, *127*, 5641; c) P. Ghosh, E. Bill, T. Weyhermüller, K. Wieghardt, *J. Am. Chem. Soc.* **2003**, *125*, 3967; d) S. Blanchard, E. Bill, T. Weyhermüller, K. Wieghardt, *Inorg. Chem.* **2004**, *43*, 2324.
- [15] a) E. Baggio-Saitovich, M. A. De Paoli, *Inorg. Chim. Acta* **1976**, *17*, 59; b) J. Blomquist, U. Helgeson, L. C. Moberg, R. Larsson, A. Mieziš, *J. Inorg. Nucl. Chem.* **1977**, *39*, 1539.
- [16] N. S. Hush, *Prog. Inorg. Chem.* **1967**, *8*, 391.
- [17] K. Chlopek, E. Bothe, F. Neese, T. Weyhermüller, K. Wieghardt, *Inorg. Chem.* **2006**, *45*, 6298.
- [18] a) A. D. Becke, *Phys. Rev. A* **1988**, *38*, 3098; b) J. P. Perdew, *Phys. Rev. B* **1986**, *33*, 8822.
- [19] J. P. Perdew, *Phys. Rev. B* **1986**, *34*, 7406.
- [20] J. P. Perdew, Y. Wang, in *Electronic Structure of Solids* (Eds.: P. Ziesche, H. Eschrig), Akademie Verlag, Berlin, **1991**.
- [21] a) A. D. Becke, *J. Chem. Phys.* **1993**, *98*, 5648; b) C. T. Lee, W. T. Yang, R. G. Parr, *Phys. Rev. B* **1988**, *37*, 785; c) P. J. Stephens, F. J. Devlin, C. F. Chabalowski, M. J. Frisch, *J. Phys. Chem.* **1994**, *98*, 11623.
- [22] See the Supporting Information for details.
- [23] a) C. Adamo, V. Barone, A. Bencini, F. Totti, I. Ciofini, *Inorg. Chem.* **1999**, *38*, 1996; b) A. P. Ginsberg, *J. Am. Chem. Soc.* **1980**, *102*, 111; c) L. Noodleman, *J. Chem. Phys.* **1981**, *74*, 5737; d) L. Noodleman, J. G. Norman, J. H. Osborne, A. Aizman, D. A. Case, *J. Am. Chem. Soc.* **1985**, *107*, 3418; e) L. Noodleman, E. R. Davidson, *Chem. Phys.* **1986**, *109*, 131; f) L. Noodleman, D. A. Case, A. Aizman, *J. Am. Chem. Soc.* **1988**, *110*, 1001; g) L. Noodleman, C. Y. Peng, D. A. Case, J. M. Mouesca, *Coord. Chem. Rev.* **1995**, *144*, 199; h) A. A. Ovchinnikov, J. K. Labanowski, *Phys. Rev. A* **1996**, *53*, 3946.
- [24] a) D. Herebian, K. E. Wieghardt, F. Neese, *J. Am. Chem. Soc.* **2003**, *125*, 10997; b) V. Bachler, G. Olbrich, F. Neese, K. Wieghardt, *Inorg. Chem.* **2002**, *41*, 4179.
- [25] P. Ghosh, E. Bill, T. Weyhermüller, F. Neese, K. Wieghardt, *J. Am. Chem. Soc.* **2003**, *125*, 1293.
- [26] a) T. Soda, Y. Kitagawa, T. Onishi, Y. Takano, Y. Shigeta, H. Nagao, Y. Yoshioka, K. Yamaguchi, *Chem. Phys. Lett.* **2000**, *319*, 223; b) K. Yamaguchi, Y. Takahara, T. Fueno, in *Applied Quantum Chemistry* (Ed.: V. H. Smith), Reidel, Dordrecht, **1986**, p. 155.
- [27] F. Neese, *J. Biol. Inorg. Chem.* **2006**, *11*, 702.
- [28] F. Neese, *J. Phys. Chem. Solids* **2004**, *65*, 781.
- [29] S. Sinnecker, L. D. Slep, E. Bill, F. Neese, *Inorg. Chem.* **2005**, *44*, 2245.
- [30] a) J. P. Simonato, J. Pecaut, L. Le Pape, J. L. Oddou, C. Jeandey, M. Shang, W. R. Scheidt, J. Wojaczynski, S. Wolowiec, L. Latos-Grazynski, J. C. Marchon, *Inorg. Chem.* **2000**, *39*, 3978; b) T. Ikeue, T. Saitoh, T. Yamaguchi, Y. Ohgo, M. Nakamura, M. Takahashi, M. Takeda, *Chem. Commun.* **2000**, 1989.
- [31] P. Gütllich, in *Mössbauer Spectroscopy, Vol. 5* (Ed.: U. Gonser), Springer, Berlin, Heidelberg, New York, **1975**, p. 53.
- [32] M. P. Hendrich, W. Gundersen, R. K. Behan, M. T. Green, M. P. Mehn, T. A. Betley, C. C. Lu, J. C. Peters, *Proc. Natl. Acad. Sci. USA* **2006**, *103*, 17107.
- [33] C. Vogel, F. W. Heinemann, J. Sutter, C. Anthon, K. Meyer, *Angew. Chem.* **2008**, *120*, 2721; *Angew. Chem. Int. Ed.* **2008**, *47*, 2681.
- [34] a) R. G. Serres, C. A. Grapperhaus, E. Bothe, E. Bill, T. Weyhermüller, F. Neese, K. Wieghardt, *J. Am. Chem. Soc.* **2004**, *126*, 5138; b) P. Gütllich, R. Link, A. Trautwein, *Mössbauer Spectroscopy and Transition Metal Chemistry*, Springer, Berlin, Heidelberg, New York, **1978**.
- [35] That is why, for instance, high-spin ferrous complexes rarely show expected from the crystal field theory $\Delta E_{O_0} \approx 4.2 \text{ mms}^{-1}$.
- [36] SHELXTL 6.14 Bruker AXS Inc., Madison, WI (USA), **2003**.
- [37] F. Neese, ORCA—an Ab Initio, Density Functional and Semiempirical Program Package, version 2.6, revision 04, Institut für Physikalische und Theoretische Chemie, Universität Bonn (Germany), July **2007**.
- [38] a) S. Grimme, *J. Comput. Chem.* **2004**, *25*, 1463; b) S. Grimme, *J. Comput. Chem.* **2006**, *27*, 1787.
- [39] A. Schafer, C. Huber, R. Ahlrichs, *J. Chem. Phys.* **1994**, *100*, 5829.
- [40] A. Schafer, H. Horn, R. Ahlrichs, *J. Chem. Phys.* **1992**, *97*, 2571.
- [41] a) E. J. Baerends, D. E. Ellis, P. Ros, *Chem. Phys.* **1973**, *2*, 41; b) B. I. Dunlap, J. W. D. Connolly, J. R. Sabin, *J. Chem. Phys.* **1979**, *71*, 3396; c) O. Vahtras, J. Almlöf, M. W. Feyereisen, *Chem. Phys. Lett.* **1993**, *213*, 514.
- [42] a) K. Eichkorn, O. Treutler, H. Ohm, M. Haser, R. Ahlrichs, *Chem. Phys. Lett.* **1995**, *242*, 652; b) K. Eichkorn, F. Weigend, O. Treutler, R. Ahlrichs, *Theor. Chem. Acc.* **1997**, *97*, 119.
- [43] a) A. T. Amos, G. G. Hall, *Proc. R. Soc. London Ser. A* **1961**, *263*, 483; b) H. F. King, R. E. Stanton, H. Kim, R. E. Wyatt, R. G. Parr, *J. Chem. Phys.* **1967**, *47*, 1936.
- [44] F. Neese, *Inorg. Chim. Acta* **2002**, *337*, 181.
- [45] a) P. O. Löwdin, *J. Chem. Phys.* **1950**, *18*, 365; b) P. O. Löwdin, *Adv. Quantum Chem.* **1970**, *5*, 185.
- [46] Portmann, S. Molekel, version 4.3.win32, CSCS/UNI Geneva, Switzerland, November **2002**.
- [47] The fit is much more sensitive to A_{xx} and A_{yy} , than to A_{zz} .
- [48] a) M. G. Gardiner, G. R. Hanson, M. J. Henderson, F. C. Lee, C. L. Raston, *Inorg. Chem.* **1994**, *33*, 2456; b) E. Rijnberg, B. Richter, K.-H. Thiele, J. Boersma, N. Veldman, A. L. Spek, G. van Koten, *Inorg. Chem.* **1998**, *37*, 56; c) P. Chaudhuri, C. N. Verani, E. Bill, E. Bothe, T. Weyhermüller, K. Wieghardt, *J. Am. Chem. Soc.* **2001**, *123*, 2213; d) M. M. Khusniyarov, K. Harms, O. Burghaus, J. Sundermeyer, *Eur. J. Inorg. Chem.* **2006**, 2985; e) J. A. Moore, A. H. Cowley, J. C. Gordon, *Organometallics* **2006**, *25*, 5207; f) N. Muresan, T. Weyhermüller, K. Wieghardt, *Dalton Trans.* **2007**, 4390; g) N. Muresan, K. Chlopek, T. Weyhermüller, F. Neese, K. Wieghardt, *Inorg. Chem.* **2007**, *46*, 5327.

Received: March 25, 2008
Published online: July 7, 2008